TO BE PUBLISHED IN THE ASTRONOMICAL JOURNAL; ACCEPTED 2007 OCTOBER 30
Preprint typeset using LaTeX style emulateapj v. 03/07/07

# SPITZER SAGE OBSERVATIONS OF LARGE MAGELLANIC CLOUD PLANETARY NEBULAE

J. L. HORA[1], M. COHEN[2], R. G. ELLIS[3], M. MEIXNER[4], R. D. BLUM[5], W. B. LATTER[6], B. A. WHITNEY[7], M. R. MEADE[8], B. L. BABLER[8], R. INDEBETOUW[9], K. GORDON[10], C. W. ENGELBRACHT[10], B.–Q. FOR[10], M. BLOCK[10], K. MISSELT[10], U. VIJH[4], C. LEITHERER[4]

*To be published in the Astronomical Journal; accepted 2007 October 30*

## ABSTRACT

We present IRAC and MIPS images and photometry of a sample of previously known planetary nebulae (PNe) from the SAGE survey of the Large Magellanic Cloud (LMC) performed with the Spitzer Space Telescope. Of the 233 known PNe in the survey field, 185 objects were detected in at least two of the IRAC bands, and 161 detected in the MIPS 24 $\mu$m images. Color-color and color-magnitude diagrams are presented using several combinations of IRAC, MIPS, and 2MASS magnitudes. The location of an individual PN in the color-color diagrams is seen to depend on the relative contributions of the spectral components which include molecular hydrogen, polycyclic aromatic hydrocarbons (PAHs), infrared forbidden line emission from the ionized gas, warm dust continuum, and emission directly from the central star. The sample of LMC PNe is compared to a number of Galactic PNe and found to not significantly differ in their position in color-color space. We also explore the potential value of IR PNe luminosity functions (LFs) in the LMC. IRAC LFs appear to follow the same functional form as the well-established [O III] LFs although there are several PNe with observed IR magnitudes brighter than the cut-offs in these LFs.

*Subject headings:* planetary nebulae: general — Magellanic Clouds — infrared: stars — stars: mass loss

## 1. INTRODUCTION

The Large Magellanic Cloud (LMC) has been important for the study of many astrophysical processes and objects because it is one of the nearest galaxies to our own, and due to its location above the Galactic plane and its favorable viewing angle (35°; van der Marel & Cioni 2001), the system can be relatively easily surveyed and many of its global properties determined. These properties are important in particular for the study of planetary nebulae (PNe). The known distance to the LMC removes the relatively large uncertainty in this parameter that affects many Galactic PNe (Hajian 2006). The distance of $\sim$ 50 kpc allows individual objects to be isolated and in some cases resolved. The effects on PNe of the lower metallicity and dust/gas mass ratio in the LMC can be explored. One can also hope to detect a large fraction of the total number of PNe in the LMC, as opposed to in the Galaxy, where confusion and extinction in the plane allow us to detect only about 10% of the PNe expected to exist (Kwok 2000; Frew & Parker 2005).

An infrared survey of the LMC called Surveying the Agents of a Galaxy's Evolution (Meixner et al. 2006, SAGE) has recently been completed using the IRAC (Fazio et al. 2004) and MIPS (Rieke et al. 2004) instruments on the Spitzer Space Telescope (Werner et al. 2004). SAGE is an unbiased, magnitude-limited survey of a $\sim 7^\circ \times 7^\circ$ region centered on the LMC. This Spitzer "Legacy" survey has provided a tremendous resource for the study of the stellar populations and interstellar medium (ISM) in the LMC. Some early results on the evolved stellar populations were given by Blum et al. (2006), who identified $\sim$32,000 evolved stars brighter than the red giant tip, including oxygen-rich, carbon-rich, and "extreme" asymptotic giant branch (AGB) stars.

In this paper we explore the properties of a sample of known PNe as revealed by the SAGE data. The catalog of 277 LMC PNe assembled by Leisy et al. (1997) from surveys that cover an area of over 100 square degrees was used for the source of positions of the PNe. Leisy et al. used CCD images and scanned optical plates to obtain accurate positions of the objects to better than $0\farcs5$. They point out that the objects are in general PN candidates, with only 139 confirmed at that time with slit spectroscopy. For simplicity we will refer to the objects in the catalog as PNe, even though this caveat still applies for many of the sources. When we began to work with the SAGE data, the Leisy et al. catalog was the largest summary list of the known PNe at the time. During the course of this work, Reid & Parker (2006) published a list of PNe in the central 25 deg$^2$ of the LMC, including 169 of the previously known objects and 460 new possible, likely, or true PNe. We will present our results here for the Leisy et al. (1997) catalog, and a future paper will include the new objects in the Reid & Parker (2006) survey.

## 2. OBSERVATIONS AND REDUCTION

The observations were obtained as part of the SAGE survey of the LMC (Meixner et al. 2006). For the IRAC data, we did not use the SAGE catalog directly since the catalog is constructed to contain point sources and some of the PNe are likely to be extended in the IRAC images. Also, when we began this work both epochs had been taken but only the epoch 1 catalog was available, so by making our own mosaics

[1] Center for Astrophysics, 60 Garden St., MS 65, Cambridge, MA 02138
[2] Radio Astronomy Laboratory, 601 Campbell Hall, University of California at Berkeley, Berkeley, CA 94720
[3] Brown University, Providence, RI 02912
[4] Space Telescope Science Institute, 3700 San Martin Way, Baltimore, MD 21218
[5] National Optical Astronomy Observatory, 950 North Cherry Ave., Tucson, AZ, 85719
[6] Caltech, NASA Herschel Science Center, MS 100–22, Pasadena, CA 91125
[7] Space Science Institute, 4750 Walnut St. Suite 205, Boulder, CO 80301, bwhitney@spacescience.org
[8] Department of Astronomy, 475 North Charter St., University of Wisconsin, Madison, WI 53706
[9] Dept. of Astronomy, University of Virginia, P.O. Box 3818, Charlottesville, VA 22903
[10] Steward Observatory, University of Arizona, 933 North Cherry Ave., Tucson, AZ 85719

using both epochs and performing the photometry we could obtain higher sensitivity and be less susceptible to instrument artifacts and cosmic rays. Using the known LMC PNe locations from the Leisy et al. (1997) catalog, all Basic Calibrated Data (BCD) images within $6'$ of the known positions were collected for inclusion in the mosaics. The SAGE survey area covered 233 of the Leisy et al. LMC PNe positions.

### 2.1. *IRAC data*

We used the version 13.2.0 BCD images as the starting point in our reduction. The 13.2.0 version of the pipeline had improved pointing reconstruction compared to previous versions, but the "DARKDRIFT" module which normalizes possible detector output channel offsets was turned off for the 3.6, 4.5, and 8.0 $\mu$m channels (it has since been turned on for BCD versions 14 and beyond). Before further processing, the "jailbar" correction algorithm[11] was applied to the BCD to remove the "pinstriping" artifact possible in this version of the data. After applying this correction, the BCD images are essentially the same as the S14 pipeline version. The images were then cleaned using custom IRAF[12] cleaning scripts to remove residual striping, banding and column pull-down artifacts. The mosaicing process removed any transient events such as cosmic rays and bad pixels as well as minimizing any fixed-pattern background noise. The BCD were combined into mosaics using the IRACproc post-BCD Processing package version 4.0 (Schuster et al. 2006). This package is based on the mopex mosaicing software released by the Spitzer Science Center (SSC) (Makovoz et al. 2006) but uses an improved outlier detection method appropriate for low coverage that rejects cosmic rays and other transients without removing pixels in the cores of real point sources. A pixel size of $0\farcs6$ and corresponding subpixel alignment of the BCD was used for the individual images to improve the resolution of the final mosaic and allow for the detection of finer structures and separation of point sources.

The IRAC photometry was extracted from these mosaics using the IRAF routines daofind and phot. The closest matching IRAC source to the Leisy et al. (1997) catalog position if less than 2 arcsec away was assumed to be the PN. In the 233 fields covered by the IRAC images, 185 PNe were detected in at least two of the IRAC bands. There were 119 sources detected in all four bands, 19 in bands 1 and 2 only, one in bands 3 and 4 only, and 24 sources detected in only one band. Since some of the fields were crowded with many point sources, a relatively small aperture size (diameter of $2\farcs8$) was used. The source crowding was more likely to affect the 3.6 and 4.5 $\mu$m images since there is significant stellar continuum emission at those wavelengths from main sequence stars. The 5.8 and 8.0 $\mu$m images were more likely to be affected by extended structured emission from the ISM in the LMC, especially in areas near star-forming regions. Having little data on the IR properties of these PNe, it is not possible to estimate on a per-object basis if a particular PN should be detectable at the sensitivity limits of the survey. An aperture correction was applied to determine the point source magnitude in the standard IRAC calibration which used a $12\farcs2$ aperture (Reach et al. 2005). Using a smaller aperture can lead to an underestimate of the nebular flux if there is significant emission outside of the aperture. However, an examination of the mosaics shows that almost all of the IRAC sources are compact and indistinguishable from other point sources in the field, so it is likely that the photometry presented here accurately represents the total emission from these objects. We have also compared our photometry for a sample of objects with photometry from the SAGE point source Catalog, which used a PSF-fitting photometry technique, and find good accord between the two different extractions, within 0.1-0.2 mag. Possible reasons for differences are that the SAGE catalog available at the time was made from the epoch 1 data only, and that if a PN is slightly extended at the IRAC resolution, it could result in fitting errors due to a poor match to the PSF.

[11] Available on the Spitzer Science Center contributed software web pages at http://ssc.spitzer.caltech.edu/irac/jailbar

[12] IRAF is distributed by the National Optical Astronomy Observatories, which are operated by the Association of Universities for Research in Astronomy, Inc., under cooperative agreement with the National Science Foundation.

TABLE 1
DETECTION STATISTICS IN EACH BAND

| Band | PNe Detected | Median Mag | Std err of median | 5 $\sigma$ sens.[a] |
|---|---|---|---|---|
| J | 39 | 15.56 | 0.37 | 17.2 |
| H | 36 | 15.30 | 0.32 | 16.2 |
| K | 42 | 14.34 | 0.27 | 15.6 |
| 3.6 | 188 | 15.59 | 0.18 | 19.3 |
| 4.5 | 197 | 15.12 | 0.17 | 18.5 |
| 5.8 | 126 | 13.33 | 0.22 | 16.1 |
| 8.0 | 157 | 12.27 | 0.20 | 15.4 |
| 24 | 161 | 7.54 | 0.20 | 10.4 |
| 70 | 18 | 2.68 | 0.67 | 3.5 |
| 160 | 0 | ··· | ··· | -0.6 |

[a] The 5-$\sigma$ point source sensitivity limits for the IRAC and MIPS data are from Meixner et al. (2006), the 2MASS limits are from the 2MASS Explanatory Supplement(Cutri et al. 2003).

### 2.2. *MIPS and 2MASS data*

The Leisy et al. (1997) positions were used to find MIPS sources from the SAGE point source catalog (Meixner et al. 2006). We found 161, 18, and 0 matching sources in the 24, 70, and 160 $\mu$m bands of the catalog, respectively. There were 109 objects detected in all four IRAC bands plus MIPS 25 $\mu$m. The large number of 24 $\mu$m detections must represent a combination of the intrinsically high sensitivity of this MIPS array, and the peak of the SED for many PNe corresponding to the characteristic temperature of $\sim$100 K for dust inside the ionized zone due to resonantly trapped Ly$\alpha$ photons. The 2MASS sources were also merged into the SAGE catalog, and those data were extracted along with the MIPS photometry from the SAGE catalog. There were 39 sources in the SAGE catalog that had corresponding 2MASS K magnitudes, and slightly fewer with J and H magnitudes.

## 3. RESULTS

The IRAC and MIPS 24 $\mu$m images for representative sources are presented in Figures 1 – 2. A summary of the number of detections in each of the survey bands and statistics on their distribution (plus 2MASS) is given in Table 1. For the 2MASS and MIPS 70 and 160 $\mu$m bands, the expected fluxes of most of the catalog PNe are below the flux limit of the survey and are undetected. In other cases, the sources might have been detected except for confusion with other sources in the field or higher background due to extended in star forming regions, for example, which will affect the statistics in those bands. The photometry results are given in Table 3. Objects are labeled in this paper as LMC n, where n is the position in the Leisy et al. (1997) catalog, from 1 to 277, and listed in column 1 of Table 3. The second column lists the distance

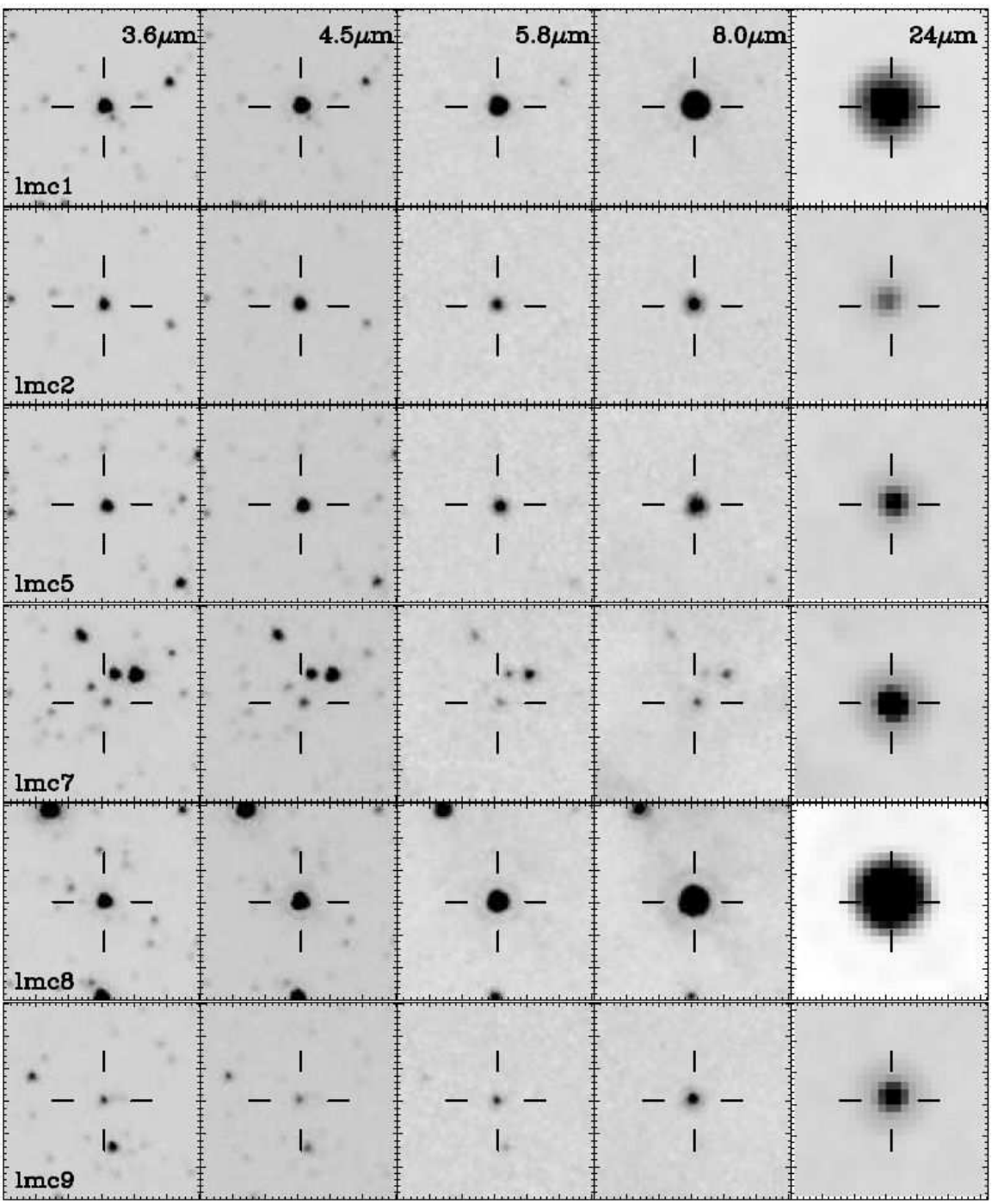


FIG. 1.—IRAC 3.6, 4.5, 5.8, and 8.0 $\mu$m and MIPS 24 $\mu$m images of nebulae imaged in the SAGE survey. Each row is labeled with the object name, and each column shows the image of that object in the different bands, labeled at the top of the figure. The images are shown with an inverse linear grayscale (brighter is darker) which is offset and scaled in each image to enhance low values near the noise level to better show faint extended emission. The images are one arcmin on a side. The crosshair lines mark the center of the field; the lines have a length of $6'$, and are separated by $18''$. This figure shows the first six objects in the survey list; figures showing all of the objects plus the FITS images of these mosaics are available at a link listed with this paper at http://www.cfa.harvard.edu/irac/publications.

in arcsec between the Leisy et al. catalog position and the IRAC source position, which was determined from the shortest wavelength band in which the object was detected. The median distance is 0.71 arcsec. Columns 3 and 4 give the position determined from the IRAC images. Columns 5 – 10 list the fluxes determined at each of the Spitzer wavelengths where the object was detected. Column 11 gives the other catalog names of the object listed by Leisy et al. (1997). Column 12 gives the characteristics of the source and field near the nebula in each band, according to the following code: A=well defined, isolated point source, B=blended with other nearby point source, C=complex background or distribution of many nearby point sources, E=extended source, N=no source visible or too faint to determine whether extended or pointlike. These categories are subjective and were assigned by two of the authors independently. Their ratings were merged by evaluating in more detail any differences. They are meant as a rough guide to the expected quality of the photometry.

Images of some representative objects[13] in the survey are shown in Figure 1. The images are presented as 1 arcmin square inverse grayscale (brighter is darker) images on a linear scale, and are centered on the Leisy et al. (1997) catalog position, indicated by the black hash marks on the images. A blank image is shown for a particular object only if it was not in the survey image at a particular band (most commonly due to its proximity to the edge of the survey field). Most of the PNe are unresolved in the IRAC and MIPS images, as the images in Figure 1 indicate. Figure 2 shows two objects with extended structure – LMC 26 and LMC 92. Due to the sometimes crowded fields and faintness of the extended emission, some of what appears to be emission from the nebulae could be from superposition of foreground or background sources unrelated to the PN. However, in the cases of LMC 26 and LMC 92, the extended emission is consistent with that observed with higher resolution optical imaging, so for those sources we have additional confidence that the IR emission is also associated with the nebula. Given the resolution of IRAC, any visible extension suggests an extent of at least 1.″2 or 0.3 pc.

### 3.1. *Color-Color and Color-Magnitude Diagrams*

Figures 3 – 7 show various color-color and color-magnitude diagrams of the datasets. In all the diagrams, the LMC sample from the SAGE data in Table 3 is plotted as red triangles, a subset of which are labeled with blue letters (not all named objects are labeled so the figure remains legible). Also plotted in the IRAC-only diagrams are data from several Galactic PNe that have been observed previously with IRAC (Hora et al. 2005; Kwok et al. 2007). The photometric data for these are given in Table 2. The underlying black points are a subsample of the SAGE catalog that have detections at least in both the 3.6 and 8.0 $\mu$m IRAC bands. Of course, to be plotted in the various diagrams, the points in addition have to be detected in all of the bands being plotted in the particular diagram. All points are plotted in each diagram if the data for those bands are available.

#### 3.1.1. *[3.6] - [4.5] versus [5.8] - [8.0]*

Figure 3 shows the four-band IRAC color-color diagram. Most SAGE sources are stars which are clustered near zero color. A broad cluster of points are centered near (1,1), and there is another sparser group extending from [5.8] - [8.0] colors of 0 to 3, and between [3.6] - [4.5] colors of 0 to 0.5. This is similar to the distribution of sources seen in large shallow surveys such as the IRAC Shallow Survey (Eisenhardt et al. 2004) where they were shown to be due to galaxies and AGN (Stern et al. 2005). However, in the LMC there are many star-forming regions and one finds many young stellar objects (YSOs; see Whitney et al. 2007) that also populate these areas of the color-color diagram, their position depending on the age of the YSO and conditions in the circumstellar disks. The LMC PNe are scattered in a region centered roughly at (1.5, 0.75), but extend all the way from objects with zero color to points near the edge of the region plotted.

The objects near (0,0) (e.g., J21 and J22) are likely dominated at these wavelengths by light from their central star. One does not expect to see many PNe near zero colors in this particular plot because of the brighter detection threshold at 8 $\mu$m compared with the other IRAC bands. However, none of the Galactic PNe are near this point, and any PN with zero colors is likely to be a highly evolved object in which the nebular gas is recombining so that other processes that are seen in the MIR are absent. These "zero color" objects appear near the main locus of stars in this and the following diagrams, except for those including wavelengths of 24 $\mu$m and beyond. Another possibility is that since several of these are in crowded regions, they could be misidentified and the photometry is for a star that is near the PN in the image.

The majority of the survey objects appear red in one or both of these colors which is likely due to either line emission from ionized gas, PAH band emission, or continuum emission from dust. In several of the objects where mid-IR spectra are available (for example, those in the Spitzer GTO observations of LMC PNe; see Bernard-Salas et al. 2004, 2005, 2006), we see that some PNe have all three of these components contributing to their emission.

#### 3.1.2. *[3.6] - [4.5] versus [4.5] - [8.0]*

In the four-band IRAC color-color diagram in Figure 3, most of the PNe are in the range of [5.8] - [8.0] colors of 1-2. Since both the 5.8 and 8 $\mu$m bands include emission from PAH features, and the strengths of the features are well correlated (Cohen et al. 1989, their Fig. 18), one might expect the PAH features to have little effect when comparing the strengths of these bands. Also, if the PN has significant warm dust continuum, it will be detected in both the 5.8 and 8.0 bands. In the [3.6] - [4.5] vs. [4.5] - [8.0] diagram shown in Figure 4, the [4.5] - [8.0] color of the PNe have a greater spread, spanning the range $\sim 1 - 4$. This could be in part due to the lack of PAH features and the much fainter emission from warm dust in the 4.5 $\mu$m band, enhancing the [4.5] - [8.0] color. In fact, one sees that several PNe with strong continuum emission from warm dust such as Hb 5, Hb 12, and SMP 76 appear at the extreme right of the PNe distribution, whereas objects with emission line spectrum and little or no dust continuum such as NGC 2440, NGC 246, and SMP83 appear on the right side of the main PNe group near (2,0.75). PNe that have strong PAH and forbidden line emission in their 5 - 15 $\mu$m spectra such as SMP 36 and SMP 38 (Bernard-Salas et al. 2005) appear on the right side but lower in the [3.6]-[4.5] color than PNe with continuum-only (in the 3-10 $\mu$m range) such as SMP 62. This bluer [3.6]-[4.5] color might reflect the contributions of the 3.3 $\mu$m PAH band and/or H recombination lines such as Pf$\gamma$ to the 3.6 $\mu$m band.

[13] The full set of images including FITS files of the IRAC and MIPS mosaics are available at a link listed with this paper at http://www.cfa.harvard.edu/irac/publications

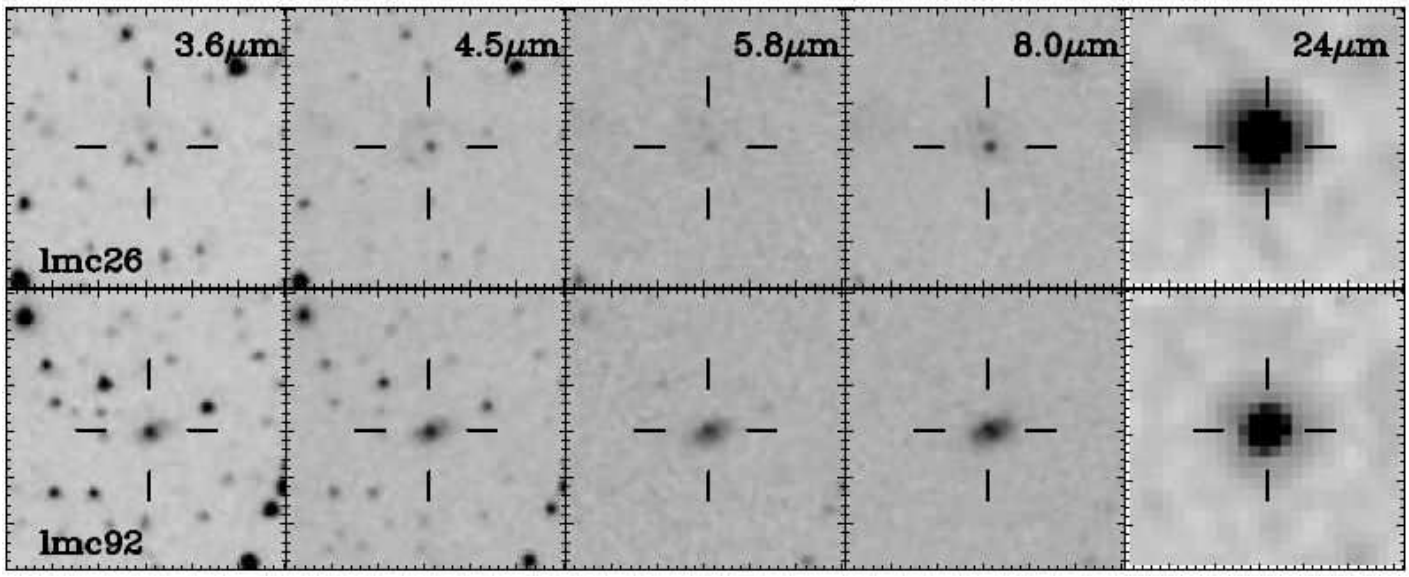


FIG. 2.—Same as Figure 1, except two PNe are plotted that show signs of extended emission.

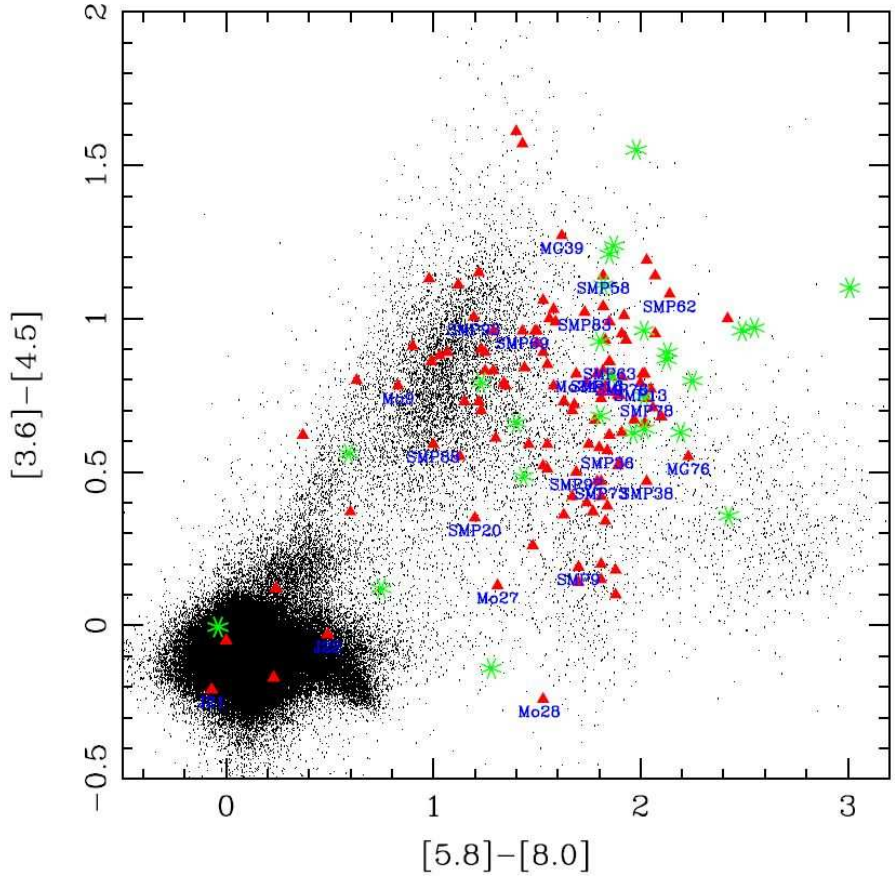


FIG. 3.—The [3.6]-[4.5] versus [5.8]-[8.0] color-color diagram for the LMC PNe and SAGE catalog sources. The LMC sample from the SAGE data in Table 3 is plotted as red triangles, and a subset of these are labeled directly below the triangles with blue letters. The subset was chosen to contain examples of different mid-IR spectral types and optically-determined morphologies. Also plotted in green are data from several Galactic PNe that have been observed previously with IRAC (Hora et al. 2005; Kwok et al. 2007, see the data in Table 2). The underlying black points are a subsample of the SAGE database that have detections at both 3.6 and 8.0 $\mu$m. All points are plotted in each diagram if the data for those bands are available.

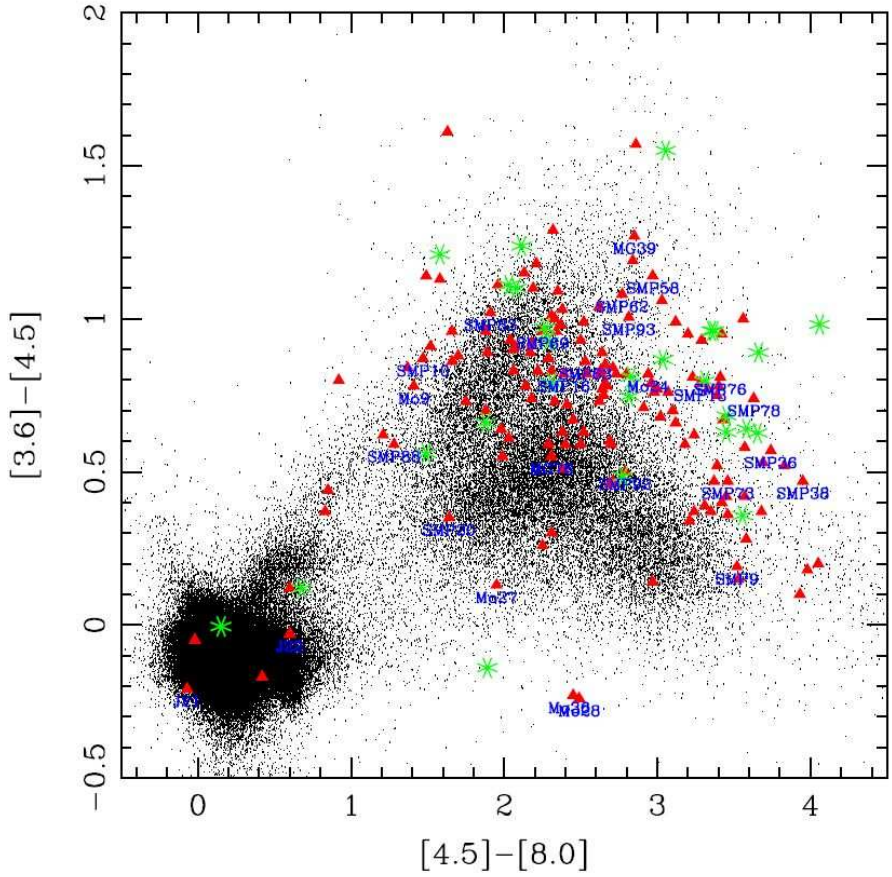


FIG. 4.—Same as Fig. 3, except the [3.6]-[4.5] versus [4.5]-[8.0] color-color diagram is plotted.

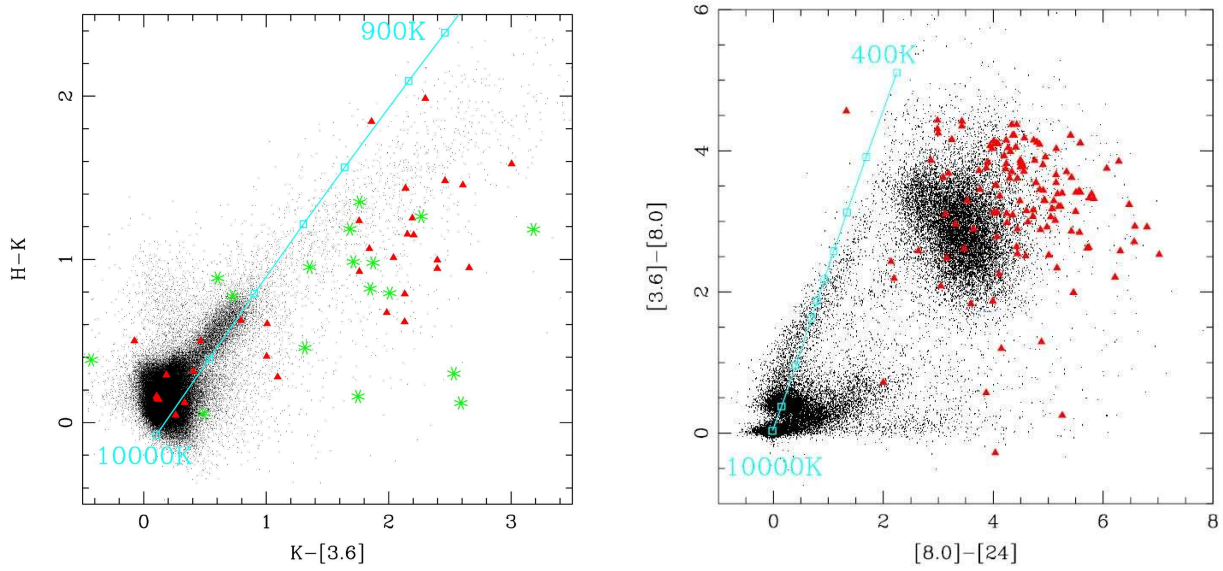


FIG. 5.—Same as Fig. 3, except the H - K versus K -[3.6] (*left*) and [3.6]-[8.0] versus [8.0]-[24] (*right*) color-color diagrams for the LMC PNe and SAGE sources. The colors of a blackbody of various temperatures are plotted in each fi gure as cyan squares connected by a line. In the fi gure on the left, temperatures of 10,000K, 3000K, 2000K, 1500K, 1250K, 1000K, 900K (from lower left to upper right) are plotted. In the fi gure on the right, temperatures of 10,000K, 3000K, 1500K, 1000K, 900K, 800K, 700K, 600K, 500K, 400K (from lower left to upper right) are plotted.

#### 3.1.3. *Near-IR to Mid-IR and Mid-IR to Far-IR color-color diagrams*

In the H - K versus K - [3.6] diagram in Figure 5, the PNe separate into two main groups, one near the locus of most of the stars near (0.2, 0.2), and the other clustered around the area near (2.2, 1.0), with a large gap in the K - [3.6] color between 1 and 2. In the first group, there is perhaps evidence for a subgroup that is slightly redder than the PNe clustered around the stellar locus at around (1.0, 0.5) in the diagram. These include SMP 62 for which the IRS spectrum shows does not show strong PAH emission, only cool dust continuum and some forbidden line emission at wavelengths longer than the IRAC bands (Bernard-Salas et al. 2005).

The colors of blackbody emission at various temperatures are plotted on the graph. Colors as red as (2.2,1.0) are characteristic of thermal emission from ∼800K dust (Allen & Glass (1974), their Fig. 2; Cohen & Kuhi (1979), their Fig. 12). Even colors of (1.0,0.5) can be caused by this mechanism although these require higher temperature grains, ∼1000K. An offset between the latter PNe and the group that is star-dominated can be understood if the materials around the PNe have condensation temperatures just above 1000K so that no hotter grains exist. Both SMP62 and SMP88, which have this putative hot dust, are dense nebulae ($N_e \sim 7000$ cm$^{-3}$: Reid 2007, private communication), consistent with local condensation of grains in clumps.

Figure 5 also shows the [3.6] - [8.0] vs. [8.0] - [24] color-color diagram. The colors of a blackbody at temperatures from 10,000K to 400K (lower left to upper right) are plotted as cyan points with a line through them. The PN population is well-separated from the distribution of main sequence stars which are clustered near the origin, and the cluster near 3000K which are likely red giant stars (Meixner et al. 2006). There is a line of cooler objects extending up the blackbody curve that is more evident here because of the larger sample of objects included in the plot. The center of the PN distribution is located above and to the right of the large number of objects centered roughly at (3,3), which are possibly extragalactic objects or YSOs (Meixner et al. 2006).

#### 3.1.4. *The [3.6] - [8.0] color-magnitude diagrams*

Figure 6 shows the [3.6] vs. [3.6] - [8.0] and the [8.0] versus [3.6] - [8.0] color-magnitude diagrams. These and the following color-magnitude diagrams show the wide range of luminosities of the PNe in the sample. The Galactic sample are plotted by adjusting their magnitudes to place them at the distance of the LMC, assuming a distance modulus of 18.5 for the LMC, and the PNe distances as given in the Strasbourg PNe catalog (Acker et al. 1992). In the [3.6] versus [3.6] - [8.0] diagram, most of the LMC PNe are roughly grouped around the position (3.5, 16). They have similar [3.6] - [8.0] colors as the Galactic sample, but the sensitivity cutoff of the SAGE survey passes roughly through the middle of the Galactic PNe distribution, indicating that we are likely not detecting a large fraction of the LMC PNe. In both of these diagrams, there are again a few PNe appearing near the distribution of LMC stars on the left side of the diagram. There are also a few bright objects that appear along the top of the diagram, with colors similar to the objects classified by Blum et al. (2006) as being "Extreme AGB" stars. One would expect that PNe could not be confused with extreme dust-shrouded AGB stars because there would be no optical spectroscopy to confirm their status as PNe. However, SMP11 is clearly an optical PN yet its MIR spectrum suggests that it is a post-AGB object (Bernard-Salas et al. 2006). Other MIR-bright PNe could likewise be in transition between post-AGB and proto-PN stages. §4 contains further discussion of these bright PNe. Most of the LMC PNe are on the right side of the diagram, near the clump of what are probably background galaxies in the SAGE catalog (see Blum et al. 2006, Figure 5). Also, the distribution of PNe are similar to the colors expected for YSOs (Whitney et al. 2007).

#### 3.1.5. *Other color-color and color-magnitude diagrams*

Figure 6 shows the [8.0] versus [3.6] - [8.0] diagram, and Figure 7 shows the [24] versus [8.0] - [24] diagram. These figures can be compared to Figures 5 and 6 of Blum et al. (2006), which labeled a few bright PNe which appeared at [8.0] - [24] colors of 3 - 5, and [24] of 1 - 2. From our Figure 7, it can be seen that the majority of PNe are in this color range, but are detected here at fainter magnitudes. There is significant overlap between the PNe and the large group of objects labeled "galaxy candidate" and "no 2MASS J" in the Blum et al. (2006) figure. However, the distribution of PNe is centered at a position brighter and slightly redder than the galaxy candidate distribution.

Figure 7 shows the [8.0] versus J - [8.0] diagram, which can be compared to Figure 4 of Blum et al. (2006). There is a set of PNe that fall slightly above the group of objects identified as galaxy candidates in Blum et al., but a larger group of objects appear at the red tip of that distribution, slightly fainter than the extreme AGB star distribution. The objects that have strong PAH and continuum dust emission, such as SMP 38 and SMP 76, appear on the red end of the distribution, whereas objects with strong ionized gas lines such as SMP 62 appear less red. This distribution is possibly due to the 6–9 $\mu$m plateau emission and the several PAH bands in the 8.0 $\mu$m IRAC band making objects like SMP 38 appear more red (Bernard-Salas et al. 2005). These strong PAH features are typical of young PNe, for example NGC 7027 (Bernard-Salas et al. 2001). In more evolved PNe, the H recombination lines dominate the near-IR emission (Hora et al. 1999). For example, the brightest near-IR line in the J band is Pa$\beta$ line at 1.28 $\mu$m. These lines could make the objects appear bluer than they would from the stellar continuum alone. The Galactic sources are at fainter [8.0] and redder J - [8.0] colors than the LMC population, falling below the sensitivity limits of the 2MASS and/or the IRAC LMC data. The difference in the distributions could be due to the fact that the Galactic sample was chosen with the criteria that they are relatively nearby objects that happen to be in the GLIMPSE and 2MASS surveys, whereas in the LMC our sensitivity limits have selected the brightest objects in that galaxy. We might find that many of the sources that are detected by IRAC but missing from the 2MASS database lie in the region indicated by the Galactic sources.

Figure 8 shows the [8.0] versus [8.0] - [24] color-magnitude diagram. The lower left corner of the diagram is blank due to the sensitivity limit of the survey in the 8.0 and 24 $\mu$m bands. The objects near zero color are stars, and a significant population of objects centered near (3.5, 13) are likely YSOs or extragalactic background objects (Meixner et al. 2006; Whitney et al. 2007). The distribution of PNe overlap with this region, but should be much less common, so it is likely that most of the other SAGE catalog objects in this range are YSOs or background objects.

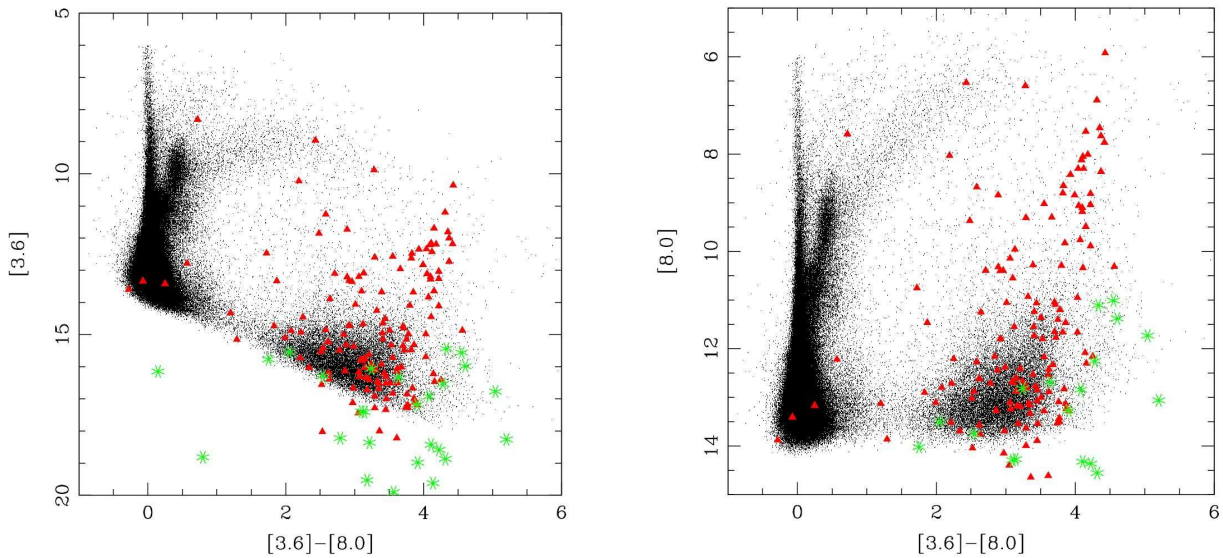


FIG. 6.—Left: Same as Fig. 3, except the IRAC [3.6] versus [3.6]-[8.0] (*left*) and [8.0] versus [3.6]-[8.0] (*right*) color-magnitude diagrams are shown. The magnitudes of the Galactic PNe were shifted to the value they would have at the distance of the LMC (see text).

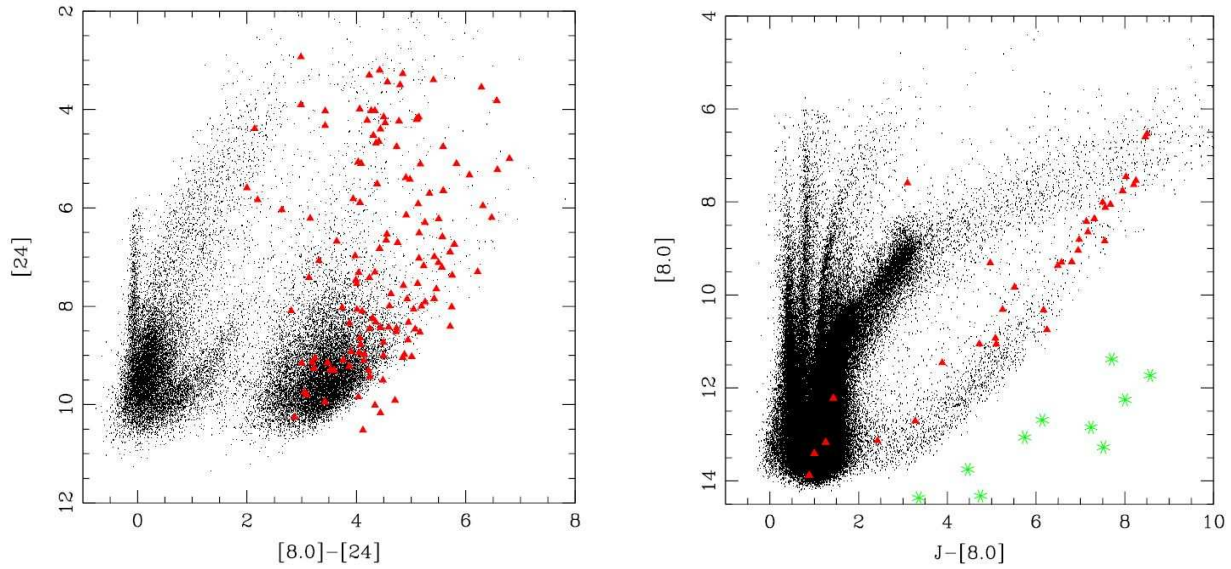


FIG. 7.—Same as Fig. 6, except the [24] versus [8.0]-[24] (*left*) and [8.0] versus J - [8.0] (*right*) color-magnitude diagrams are shown.

### 3.2. *Planetary Nebulae Spectral Energy Distributions*

Two examples of Spectral Energy Distributions (SEDs) are shown in Figure 9. The SEDs have been normalized in each plot to the 3.6 $\mu$m flux of the objects specified in the figure, in order to easily compare the SED shapes. In the top plot of Figure 9 the SEDs of all of the PNe that were detected by 2MASS and in the 70 $\mu$m MIPS channel are plotted, in order to show the widest wavelength range possible in the dataset. The sensitivity limit of the 70 $\mu$m data is near the 20 mJy level of the lowest plotted point. The requirement of a 70 $\mu$m detection has selected objects with similar SEDs.

In the bottom plot of Figure 9, the 70 $\mu$m requirement was dropped and a selection of sources were plotted that have 2MASS, IRAC, and 24 $\mu$m detections (there were 29 such sources in total). Here the greater diversity of SEDs is seen that is also reflected in the color-color and color-magnitude diagrams shown above. With only one exception in this subsample (MG 47), all of the PNe show a rise between 8-24 $\mu$m indicating a cool dust component. There were a total of 26 sources in this group of objects with 24 $\mu$m flux larger than the 8 $\mu$m flux, or roughly 90%. The objects with 8 $\mu$m larger than the 24 $\mu$m flux may belong to a different class of PNe, perhaps having a warmer dust component that dominates the IR luminosity. The 24 $\mu$m data are not available for the Galactic sources in our sample to compare to the LMC sample.

The minimum in the SED varies from 8 $\mu$m down to the J band, and is likely influenced by the relative strengths of the stellar continuum and scattered light in the near-IR, $H_2$ emission and warm dust emission in the IRAC bands, PAH emission that can enhance the 5.8 and 8.0 $\mu$m emission, cooler dust in the 24 $\mu$m band, and forbidden line emission from the ionized gas which could affect multiple bands.

### 3.3. *Individual Planetary Nebulae*

Figure 2 shows two PNe in the catalog that have clearly resolved extended emission in the IRAC images. These are discussed in the sections below.

TABLE 2
GALACTIC PLANETARY NEBULA MAGNITUDES

| Name | J | H | K | [3.6] | [4.5] | [5.8] | [8.0] |
|---|---|---|---|---|---|---|---|
| Hubble 12 | ... | ... | ... | 6.94 | 5.98 | 5.1 | 2.61 |
| NGC 2440 | 10.33[a] | 10.50 | 9.68 | 7.83 | 7.02 | 6.05 | 4.19 |
| NGC 246 | ... | ... | ... | 8.91 | 7.8 | 7.59 | 5.77 |
| NGC 650 | ... | ... | ... | 9.72 | 8.51 | 8.78 | 6.93 |
| NGC 3132 | 9.71[a] | 9.70 | 9.54 | 7.79 | 7.13 | 6.65 | 5.25 |
| NGC 6543 | ... | ... | ... | 7.56 | 6.59 | 6.87 | 4.32 |
| Hubble 5 | ... | ... | ... | 7.06 | 6.17 | 4.64 | 2.51 |
| IC 4406 | ... | ... | 10.1[b] | 8.89 | 8.1 | 7.02 | 5.79 |
| PNG 002.7-52.4 | ... | ... | ... | 11.03 | 9.93 | 10.86 | 7.85 |
| Mz 1 | ... | ... | ... | 7.27 | 7.41 | 6.8 | 5.52 |
| NGC 2346 | ... | ... | ... | 7.05 | 6.49 | 5.59 | 5 |
| G010.1045+00.7414[c] | 10.589 | 10.181 | 9.196 | 7.48 | 5.93 | 4.86 | 2.88 |
| G011.7469-00.6475 | 11.759 | 11.561 | 10.298 | 8.03 | 7.40 | 5.72 | 3.75 |
| G035.5650-00.4910 | 13.019 | 11.360 | 10.585 | 9.86 | 8.93 | 8.45 | 6.64 |
| G055.5077-00.5558 | 11.582 | 11.276 | 10.297 | 8.42 | 7.79 | 6.54 | 4.34 |
| G056.4016-00.9032 | 14.205 | 13.712 | 12.760 | 11.41 | 10.66 | 9.86 | 7.84 |
| G062.4909-00.2698 | 15.325 | 14.584 | 14.464 | 11.87 | 10.64 | 10.40 | 8.52 |
| G300.2818+00.6619 | 10.569 | 10.473 | 10.417 | 9.93 | 9.13 | 8.07 | 5.82 |
| G300.4289-00.9815 | 15.282 | 13.648 | 13.190 | 11.87 | 11.39 | 10.05 | 8.61 |
| G302.3730-00.5390 | 14.287 | 13.954 | 13.654 | 11.12 | 10.44 | 8.79 | 6.99 |
| G306.4740+00.2590 | 10.500 | 10.271 | 9.887 | 10.32 | 10.20 | 10.27 | 9.52 |
| G315.0266-00.3744 | 15.221 | 14.735 | 13.552 | 10.37 | 9.41 | 8.07 | 6.05 |
| G318.9300+00.6930 | 14.988 | 13.285 | 12.492 | 10.48 | 10.13 | 9.00 | 6.57 |
| G321.0230-00.6990 | 9.216 | 8.722 | 8.375 | 10.08 | 9.44 | 7.88 | 5.86 |
| G322.4700-00.1800 | 11.805 | 11.142 | 9.956 | 8.27 | 7.29 | 6.46 | 3.23 |
| G333.9279+00.6858 | 10.306 | 9.235 | 8.475 | 9.76 | 7.00 | 7.09 | 4.56 |
| G342.7456+00.7521 | 11.121 | 9.137 | 8.252 | 7.65 | 7.65 | 7.46 | 7.50 |
| G343.9923+00.8355 | 12.292 | 11.791 | 10.440 | 8.68 | 7.81 | 6.90 | 4.77 |

[a] JHK data from Whitelock (1985), using a 24" aperture.
[b] K data from Allen & Glass (1974)
[c] Data for all objects starting with "G" are from Kwok et al. (2007). Note that the JHK magnitudes are from the 2MASS point source catalog, so they might be underestimates of the total flux from the central star plus nebula.

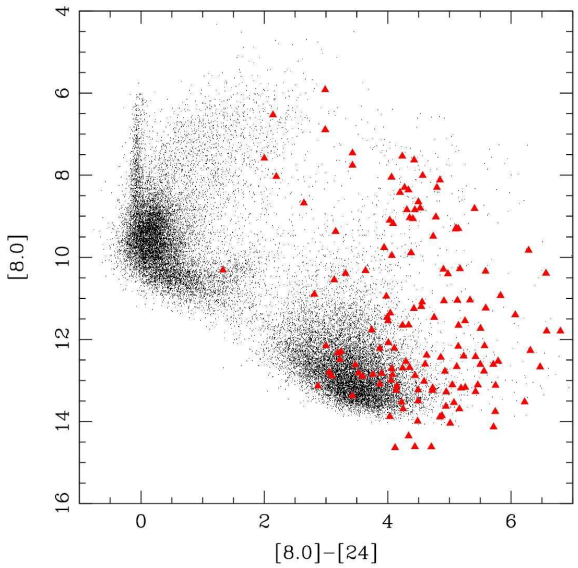


FIG. 8.—Same as Fig. 3, except the [8] versus [8.0]-[24] color-magnitude diagram is shown.

### 3.3.1. *LMC 26 (SMP 27)*

A very large faint halo is visible at a distance of $\sim 7''$ from the core in the IRAC images. Shaw et al. (2001) also detected an arc visible at $6''.25$ to the northwest in HST images, and hypothesized that the largest outer arc consists of remnants of the giant branch star that preceded the nebula. Shaw et al. also detect a compact quadrupolar nebula around the central star that is too small to be resolved in the IRAC images. However the arcs can be seen in the IRAC images to extend much further around the star than in the HST images. The arcs are traceable at 4.5 $\mu$m as an almost complete ring, particularly on the eastern side of the central nebula, and more diffuse emission is visible completely surrounding the object in the 8.0$\mu$m image.

### 3.3.2. *LMC 92 (SMP 93)*

The PN appears bipolar in the IRAC images, with a bright core and two distinct lobes extending to the northwest and southeast. The MIPS resolution is not sufficient to resolve the nebula, but an elongation is apparent in the 24 $\mu$m image at the same position angle. The infrared structure is consistent with that seen by Shaw et al. (2001) in their HST image, which they determined to have a maximum extent of $6''.4$ or 1.57 pc. The lobes are brighter relative to the core at the longer IRAC wavelengths.

## 4. LMC PN LUMINOSITY FUNCTION

PNe in the Magellanic Clouds and in more distant galaxies follow a universal form of [O III] luminosity function (LF) which is thought to arise because [O III] is the dominant optical coolant (Jacoby 1989; Ciardullo et al. 1989). The absolute [O III] magnitude corresponding to the sharp PN luminosity function (PNLF) cut-off is now regarded as among the best standard candles for cosmology (Jacoby et al. 1990; Ciardullo 2005; Jacoby et al. 2006). It would be of interest to know whether LMC PNe reveal any IR analogs to the optical character of the LFs because a cosmological distance scale based on an IR standard candle would be a potent tool for determin-

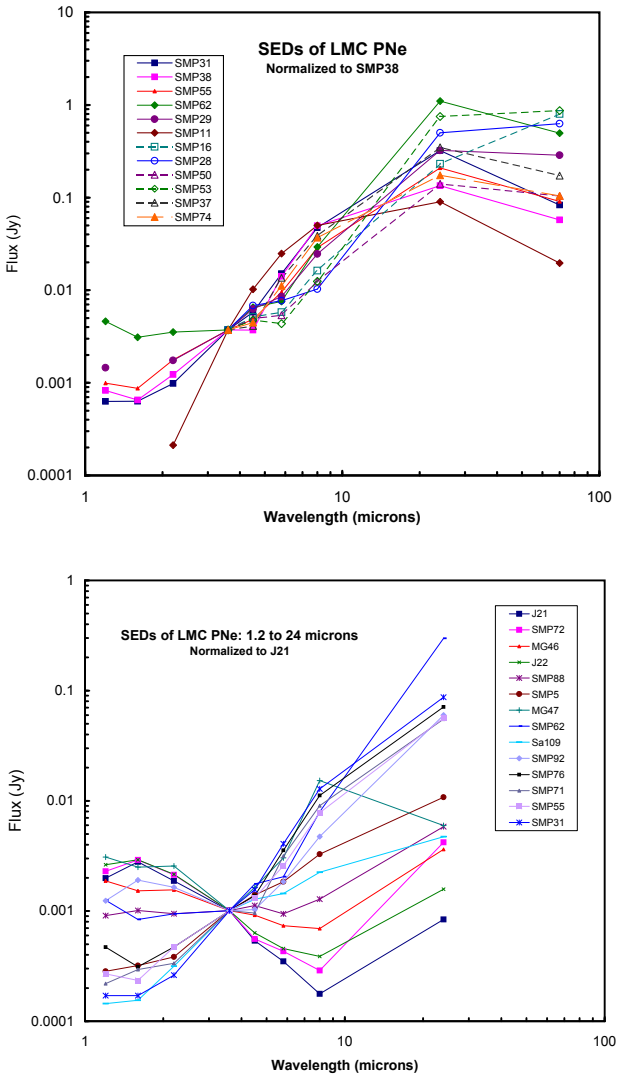


FIG. 9.—Planetary nebulae SEDs. (Top) SEDs from 1.2 - 70 $\mu$m. The SEDs have been normalized to the 3.6 $\mu$m flux of SMP 38. (Bottom) SEDs from 1.2 - 24 $\mu$m. The SEDs have been normalized to the 3.6 $\mu$m flux of J21.

ing distances of optically invisible dusty galaxies. Therefore, we have investigated whether the function by Jacoby (1989) also fits the histograms of IR magnitudes for LMC PNe.

Henize & Westerlund (1963) first constructed a PNLF adopting a constant-mass, uniformly expanding model for a PN whose central star did not evolve. They also advanced the concept that PNe in different galaxies attain the same maximum brightness. The LF is an integrated snapshot of an evolving ensemble of central stars of different mass and their associated evolving nebulae. Ciardullo et al. (1989) modified this expanding and slowly dimming model to explain the sharp turn-down observed at the bright end of M31's PNLF. They included an exponential truncation to represent a cut-off in the upper mass limit of PN central stars, and stellar evolution that is strongly mass-dependent. The same function still suffices to represent PNLFs in the many galaxies for which a LF for the 5007Å [O III] line (or an H$\alpha$ or H$\beta$ LF) has been built (e.g., Frew & Parker 2006). Optical PNLF histograms are fit by the function $N(M)=e^{0.307M}(1-e^{3(M^*-M)})$ where M is the equivalent [O III] magnitude and $M^*$ the absolute 5007Å magnitude of the brightest PN that can exist in any galaxy. $M^*=-4.47\pm0.05$ and this is the [O III] standard candle. In fact $M^*$ depends slightly on metallicity. Rigorous testing has shown it to be fainter in metal-poor galaxies but constant for galaxies whose [O/H] abundance is above that of the LMC (Ciardullo 2005).

Ciardullo & Jacoby (1999) argued from the initial-mass-final mass-relation that high-mass central stars must have massive circumstellar envelopes from which dust cannot escape during the rapid changes in stellar conditions. Thus a PN around a massive central star will always suffer strong internal extinction, diminishing its observed line flux, perhaps even preventing its optical detection. Ciardullo (2006) commented that although no PN is observed above the [O III] bright cut-off, PNe are certainly known with true fluxes about twice that corresponding to $M^*$. If the optical cut-off were due to the combination of massive progenitors suffering internal nebular extinction, then one would expect to observe IR LFs with PNe brighter than any analogous IR cut-off because our LFs correspond to wavelengths at which extinction is far smaller than at 5007Å. This is a prediction that we can test.

PNe appear to emit in the IR by any or all of several possible mechanisms. It is not obvious that they should mimic the behavior modeled for the evolution of [O III] and H$\alpha$ emission. However, the fluorescence of PAH bands, fine structure line radiation, and optically-thin thermal dust emission are processes linked to stellar luminosity, particularly UV flux. Therefore, MIR luminosity in a PN may well track the variations in stellar UV luminosity. All PNe undergo an initial expansion and their central stars are of low or intermediate mass, implying a declining mass spectrum in their progenitor population. Only for edge-on disk geometries would the MIR emission of a PN also depend on the viewing angle and these are associated with the roughly 10% of all PNe that are Type 1 N-rich bipolar PNe and have the highest mass central stars. Consequently, an initial exploration of the LMC infrared PNLFs is worthwhile.

Our magnitude samples are too sparse in the near-infrared and at 70 $\mu$m but we present LFs in all IRAC bands and at 24 $\mu$m in Figure 10. We found that 0.5 magnitude bins are too small to remove the noise but 0.75 magnitude appears to average out inappropriately high frequency structure while preserving essential features. Each of the IRAC LFs was fitted independently to the identical truncated exponential form used by Jacoby and colleagues (equation 2 of Ciardullo et al. 1989). The function was scaled by least squares minimization to best match the observed counts in the domain from the obvious cut-off to the estimated limit of completeness (the vertical dashed lines in these figures). Each IRAC LF resembles the optical LFs structurally in that we see cut-offs near magnitudes of 9.5, 9.5, 8.5 and 6.6 in IRAC bands 1–4, respectively. We also note possible "Jacoby" dips near [3.6]=14.5, [4.5]=13.5, [5.8]=12.0 and [8.0]=10.5, where the counts fall about a factor of 2 below the exponential. Any unpopulated regions in a PNLF are attributed to populations in which central star evolution proceeds very rapidly (Jacoby & de Marco 2002). The IRAC PNLFs appear promising, with IR analogs of the bright end cut-offs observed in optical emission lines. The quantitative connections between these IR magnitudes and the [O III] $M^*$ will be the subject of a future detailed study.

Of particular importance are those objects brighter than the cut-offs. They may not all be PNe. Spuriously matched field

stars, symbiotic objects, and H II regions are the typical contaminants of PNLFs in several wavelength regimes. An inventory of all PNe that are brighter than the cut-off at any IRAC wavelength shows only 6 different objects. These are LMC numbers 123, 125, 11, 63, 35, and 231, ordered from most to least frequently encountered brighter than $M^*$. Information on the characteristics of these PNe from Leisy et al. (1997) and Reid & Parker (2006) is somewhat sparse but indicates that all are in the LMC (from radial velocities), and that LMC 63 is regarded only as a "possible PN" by Reid & Parker because of its very-low excitation spectrum. LMC11 (SMP11) is more likely to be a post-AGB object or a proto-PN rather than a typical PN. At present we cannot eliminate any of the other 4 objects as being non-PNe or transitional objects. If any of these outlying PNe in our LFs survive further scrutiny then this would validate the suggestion of heavy internal extinction in PNe with high-mass central stars.

We can offer no clear interpretation for the 24 $\mu$m LF. Although it looks superficially to mimic the universal optical form, our best-fitting truncated exponential falls well below what appears to be a second peak in the LF near [24]=3.5. If we regard this as due to a LF dip near [24]=6 then it would argue for a far higher exponential contribution than the observed counts support. It is also possible that the secondary 24 $\mu$m peak represents all the optically extinguished PNe beyond the [O III] cut-off that are now observable because of either the negligible extinction at this long wavelength or the re-emission in the MIR of internally absorbed optical luminosity.

## 5. CONCLUSIONS

We have presented images and photometry of the Leisy et al. (1997) sample of PNe in the LMC. Of the 233 known PNe in the survey field, 185 objects were detected in at least two of the IRAC bands, and 161 detected in the MIPS 24 $\mu$m images. Color-color and color-magnitude diagrams were presented using several combinations of IRAC, MIPS, and 2MASS magnitudes. The location of an individual PN in the color-color diagrams was seen to depend on the relative contributions of the spectral components, resulting in a wide range of colors for the objects in the sample. A comparison to a sample of Galactic PNe shows that they do not substantially differ in their position in color-color space. The location of PNe in the various infrared color-color and color-magnitude diagrams are in general well separated from normal stars, but overlap significantly with extragalactic sources and potential YSOs. Any ambiguity between PNe and YSOs or galaxies can be readily resolved by the unique optical characteristics of PNe and their environs. Therefore, an IR color-based search for new PNe in the LMC would be viable in combination with deep optical imaging and spectroscopy. The latter remains the prerequisite to confirm a candidate as a PN.

We have offered an exploration of the potential value of IR PNLFs in the LMC. IRAC LFs appear to follow the same functional form as the well-established [O III] LFs although there are several PNe with observed IR magnitudes brighter than the cut-offs in these LFs. If these objects can be demonstrated to be true PNe and not very-low excitation variants nor symbiotic stars then their existence may confirm the long-standing suggestion that PNe with massive central stars suffer heavy internal extinction. This extinction would eliminate optical outliers beyond the cut-off magnitude but would affect IR LF counts minimally so that all such outliers could be observed.

This work is based in part on observations made with the Spitzer Space Telescope, which is operated by the Jet Propulsion Laboratory, California Institute of Technology under NASA contract 1407. Support for this work was provided by NASA through Contract Number 1256790 issued by JPL/Caltech. Support for the IRAC instrument was provided by NASA through Contract Number 960541 issued by JPL. This work is based in part on the IRAC post-BCD processing software "IRACproc" developed by Mike Schuster, Massimo Marengo and Brian Patten at the Smithsonian Astrophysical Observatory. MC thanks NASA for supporting his participation in SAGE through JPL contract number 1275471 with UC Berkeley. This work made use of the Two Micron All Sky Survey (2MASS) database, which is a joint project of the University of Massachusetts and the Infrared Processing and Analysis Center/California Institute of Technology, funded by the National Aeronautics and Space Administration and the National Science Foundation. This research has made use of the VizieR catalogue access tool and the SIMBAD database, CDS, Strasbourg, France.

## REFERENCES

Acker, A., Ochsenbein, F., Stenholm, B., Tylenda, R., Marcout, J., Schohn C., 1992, Strasbourg-ESO Catalogue of Galactic Planetary Nebulae, (Garching: European Southern Observatory)
Allen, D. A., & Glass, I. S. 1974, MNRAS, 167, 337
Bernard-Salas, J., Pottasch, S. R., Beintema, D. A., & Wesselius, P. R. 2001, å, 367, 949
Bernard-Salas, J., Peeters, E., Sloan, G. C., Cami, J., Guiles, S., Houck, J. R. 2004, ApJS, 154, 271
Bernard-Salas, J., Houck, J. R., Pottasch, S. R., Peeters, E. 2005, in Planetary Nebulae as Astronomical Tools, eds. R. Szczerba, G. Stasińska, & S. K. Górny, AIP Conf. Proc. 804, 56
Bernard-Salas, J., Peeters, E., Sloan, G. C., Cami, J., Guiles, S., Houck, J. R. 2006, ApJ, 652, L29
Blum, R. D. et al. 2006, AJ, 132, 2034
Ciardullo, R. & Jacoby, G. H. 1999, ApJ, 515, 19
Ciardullo, R. 2005, AIP Conference Proceedings, 804, 277
Ciardullo, R. 2006, in Planetary Nebulae in our Galaxy and Beyond, IAU Symp. #234., eds. M. J. Barlow & R. H. Méndez, 325
Ciardullo, R., Jacoby, G. H., Ford, H. C., & Neill, J. D. 1989, ApJ, 339, 53
Cohen, M. & Kuhi, L.V. 1979, ApJS, 41, 743
Cohen, M., Tielens, A. G. G. M., Bregman, J., Witteborn, F. C., Rank, D. M., Allamandola, L. J., Wooden, D, Jourdain de Muizon, M. 1989, ApJ, 341, 246
Cutri, R. M. et al., Explanatory Supplement to the 2MASS All-Sky Data Release (Washington, NASA), http://www.ipac.caltech.edu/2mass/releases/allsky/doc/explsup.html
Eisenhardt, P. R. et al. 2004, ApJS, 154, 296
Fazio, G. G., et al. 2004, ApJS, 154, 10
Frew, D. J. & Parker, Q. A. 2005, in Planetary Nebulae as Astronomical Tools, AIP Conf. Proc. 804, eds. R. Szczerba, G. Stasińska, & S. K. Górny, 11
Frew, D. J. & Parker, Q. A. 2006, in Planetary Nebulae in our Galaxy and Beyond, IAU Symp. #234., eds. M. J. Barlow & R. H. Méndez, 49
Hajian, A. R. 2006, in Planetary Nebulae in our Galaxy and Beyond, IAU Symp. 234, eds. M. J. Barlow & R. H. Méndez, 41
Henize, K. G & Westerlund, B. E. 1963, ApJ, 137, 747
Hora, J. L., Latter, W. B., & Deutsch, L. K. 1999, ApJS, 124, 195
Hora, J. L., Latter, W. B., Allen, L. E., Marengo, M., Deutsch, L. K., & Pipher, J. L. 2004, ApJS, 154, 296
Hora, J. L., Latter, W. B., Marengo, M., Fazio, G. G., Allen, L. E., & Pipher, J. L. 2005, BAAS, 206, 39.01
Jacoby, G. H. & de Marco, O. 2002, AJ, 123, 269
Jacoby, G. H. 1980, ApJS, 42, 1
Jacoby, G. H. 1989, ApJ, 339, 39
Jacoby, G. H., Walker, A. R. & Ciardullo, R. 1990, ApJ, 365, 471
Jacoby, G. H., Phillips, M. M., & Feldmeier, J. J. 2006, in Planetary Nebulae in our Galaxy and Beyond, IAU Symp. #234., eds. M. J. Barlow & R. H. Méndez, 435

Kwok, S. 2000, The Origin and Evolution of Planetary Nebulae (Cambridge: Cambridge University Press)
Kwok, S. et al. 2007, ApJS, in press
Leisy, P., Dennefeld, M., Alard, C., & Guibert, J. 1997, A&A, 121, 407
Makovoz, D., Roby, T., Khan, I., Booth, H. 2006, Proc. SPIE, 6274, 10
Meixner, M. et al. 2006, AJ, 132, 2268
Morgan, D. H. & Good, A. R. 1992, A&AS, 92, 571
Morgan, D. H. 1994, A&AS, 103, 235
Reach, W. et al. 2005, PASP, 117, 978
Reid, W. A., & Parker, Q. A. 2006, MNRAS, 373, 521
Rieke, G. H. et al., 2004, ApJS, 154, 25
Sanduleak, N., MacConnell, D. J., & Phillip, A. G. D. 1978, PASP, 90, 621
Sanduleak, N. 1984, in Structure and Evolution of the Magellanic Clouds, IAU Symp. #108, eds. S. van den Bergh & K. S. de Boer, 231
Schuster, M. T., et al. 2006, Proc. SPIE, 6270-74
Stern, D. et al. 2005, ApJ, 631, 163
Shaw, R. A. et al. 2001, ApJS, 548, 727-48
van der Marel, R., & Cioni, M.-R. L. 2001, AJ, 122, 1807
Werner, M. W. et al., 2004, ApJS, 154, 1
Whitelock, P. A. 1985, MNRAS, 213, 59
Whitney, B. A. et al., 2007, submitted

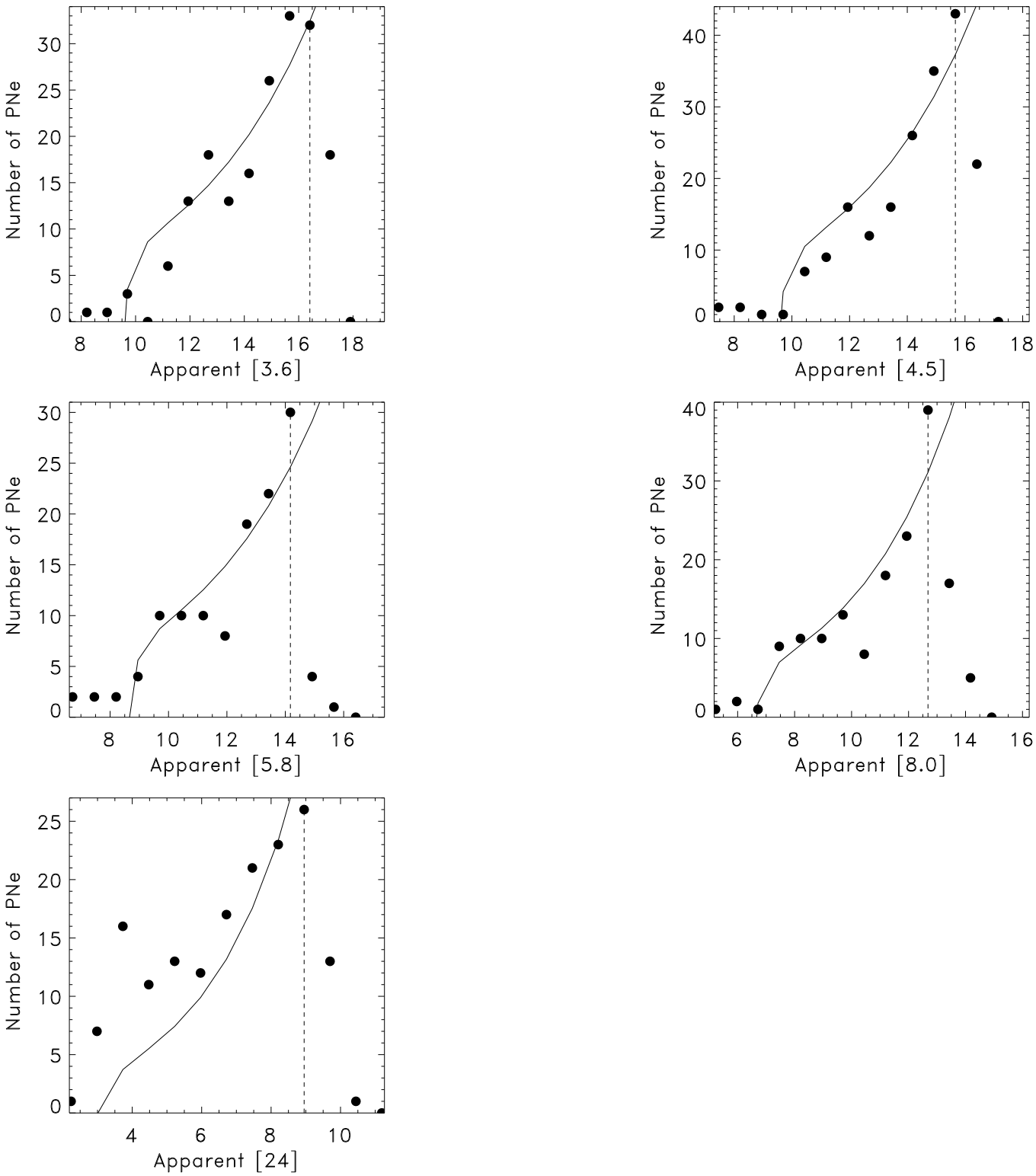


FIG. 10.—The planetary nebulosity luminosity functions for each of the IRAC channels and the MIPS 24 $\mu$m band. The vertical dashed line is the estimated completeness magnitude in each of the bands.

TABLE 3
SAGE LMC PLANETARY NEBULAE PHOTOMETRY

| LMC | Dist.[a] (arcsec) | R.A. (J2000) | Dec. (J2000) | [3.6] (err) | [4.5] (err) | [5.8] (err) | [8.0] (err) | [24] (err) | [70] (err) | Other names | Code[b] |
|---|---|---|---|---|---|---|---|---|---|---|---|
| 1 | 0.18 | 4:38:34.8 | -70:36:43.3 | 12.34 (0.01) | 11.53 (0.01) | 10.16 (0.01) | 8.30 (0.00) | 4.03 (0.01) | 3.28 (0.11) | SMP1 | AAAAA |
| 2 | 0.74 | 4:40:56.7 | -67:48:01.6 | 13.65 (0.02) | 12.73 (0.02) | 12.05 (0.02) | 10.55 (0.01) | 7.42 (0.04) | ··· | SMP2 | AAAAA |
| 5 | 1.2 | 4:48:08.7 | -67:26:06.3 | 13.21 (0.02) | 12.38 (0.01) | 11.61 (0.01) | 10.32 (0.01) | 6.68 (0.03) | ··· | SMP5 | AAAAA |
| 7 | 0.75 | 4:48:29.7 | -69:08:12.6 | 14.85 (0.04) | 14.15 (0.03) | 13.50 (0.03) | 12.27 (0.03) | 5.96 (0.02) | ··· | SMP7 | AAAAR |
| 8 | 0.56 | 4:50:13.2 | -69:33:56.6 | 12.21 (0.01) | 11.15 (0.01) | 9.65 (0.01) | 8.12 (0.00) | 3.27 (0.01) | ··· | SMP8 | AAAAA |
| 9 | 0.7 | 4:50:24.7 | -68:13:16.0 | 14.80 (0.03) | 14.61 (0.04) | 12.79 (0.02) | 11.09 (0.01) | 6.53 (0.04) | ··· | SMP9 | AAAAA |
| 10 | 0.55 | 4:51:09.0 | -68:49:05.4 | 16.03 (0.07) | 15.16 (0.05) | ··· | 13.69 (0.07) | 8.53 (0.05) | ··· | SMP10 | AAAAA |
| 11 | 0.62 | 4:51:37.9 | -67:05:16.3 | 10.35 (0.00) | 8.78 (0.00) | 7.35 (0.00) | 5.92 (0.00) | 2.94 (0.01) | 2.22 (0.09) | SMP11 | AAAAA |
| 12 | 0.28 | 4:52:01.5 | -68:39:16.9 | 16.45 (0.08) | 15.45 (0.06) | 14.68 (0.08) | 13.12 (0.05) | 7.37 (0.04) | ··· | SMP12 | AAAAA |
| 13 | 1.41 | 5:00:00.2 | -70:27:40.5 | 13.83 (0.02) | 13.04 (0.02) | 11.76 (0.01) | 9.76 (0.01) | 5.82 (0.03) | ··· | SMP13 | AAAAA |
| 14 | 0.72 | 5:00:20.8 | -70:58:50.9 | 16.87 (0.09) | 16.01 (0.08) | ··· | ··· | 8.82 (0.06) | ··· | SMP14 | AAAAA |
| 15 | 1.06 | 5:00:52.7 | -70:13:39.8 | 13.68 (0.02) | ··· | ··· | ··· | 4.76 (0.02) | ··· | SMP15 | AAAAA |
| 16 | 0.89 | 5:02:02.0 | -69:48:53.6 | 15.62 (0.05) | 14.80 (0.04) | 14.20 (0.05) | 12.41 (0.03) | 7.18 (0.04) | 3.47 (0.14) | SMP16 | CCCAA |
| 17 | 0.42 | 5:02:52.4 | -69:20:53.3 | 14.87 (0.04) | 13.88 (0.03) | 12.95 (0.02) | 11.36 (0.02) | 7.32 (0.04) | ··· | SMP17 | AAAAA |
| 18 | 0.76 | 5:03:42.7 | -70:06:46.8 | 15.37 (0.05) | 14.78 (0.04) | 13.93 (0.05) | 12.38 (0.04) | 7.75 (0.05) | ··· | SMP18 | BBAAA |
| 19 | 0.58 | 5:03:41.3 | -70:13:53.0 | 14.09 (0.03) | 13.39 (0.02) | 11.96 (0.01) | 10.29 (0.01) | 5.39 (0.03) | ··· | SMP19 | AAAAA |
| 20 | 0.48 | 5:04:40.1 | -69:21:39.6 | 15.10 (0.04) | 14.75 (0.04) | 14.31 (0.06) | 13.11 (0.04) | 7.65 (0.04) | ··· | SMP20 | BBAAA |
| 21 | 1.81 | 5:04:52.1 | -68:39:08.6 | 14.45 (0.03) | 13.46 (0.02) | 12.19 (0.02) | 10.34 (0.01) | 4.76 (0.02) | 1.78 (0.06) | SMP21 | AAAAA |
| 22 | 0.89 | 5:05:50.7 | -69:02:31.1 | 15.64 (0.06) | 15.23 (0.06) | ··· | ··· | 9.13 (0.09) | ··· | SMP22 | CCCCA |
| 24 | 1.24 | 5:06:18.3 | -68:59:30.9 | 17.05 (0.13) | 16.25 (0.10) | ··· | ··· | 8.77 (0.05) | ··· | SMP24 | NNNAA |
| 25 | 0.19 | 5:06:23.9 | -69:03:19.3 | 12.57 (0.01) | 12.23 (0.01) | 10.85 (0.01) | 9.02 (0.01) | 4.24 (0.01) | ··· | SMP25 | AAAAA |
| 26 | 0.47 | 5:07:54.9 | -66:57:45.3 | 16.04 (0.06) | 15.33 (0.05) | 14.48 (0.06) | 12.42 (0.03) | 7.00 (0.04) | ··· | SMP27 | EEEEA |
| 27 | 1.51 | 5:07:57.7 | -68:51:46.2 | 13.10 (0.02) | 11.97 (0.01) | 11.37 (0.01) | 10.39 (0.01) | 3.82 (0.02) | 1.21 (0.06) | SMP28 | AAAAA |
| 28 | 1.0 | 5:08:03.5 | -68:40:16.3 | 12.96 (0.02) | 11.92 (0.01) | 11.12 (0.01) | 9.30 (0.01) | 4.16 (0.01) | 1.92 (0.08) | SMP29 | BBBAA |
| 29 | 0.25 | 5:09:10.6 | -66:53:38.2 | 16.31 (0.07) | 15.20 (0.05) | 14.36 (0.06) | 13.24 (0.05) | 8.52 (0.05) | 3.32 (0.13) | SMP30 | AAAAA |
| 30 | 0.73 | 5:09:20.2 | -67:47:24.3 | 12.00 (0.01) | 11.05 (0.01) | 9.54 (0.00) | 7.63 (0.00) | 3.20 (0.01) | 2.30 (0.06) | SMP31 | AAAAA |
| 31 | 0.74 | 5:09:37.2 | -70:49:08.1 | 14.65 (0.03) | 13.62 (0.02) | 12.82 (0.02) | 11.24 (0.02) | 5.65 (0.03) | ··· | SMP32 | AAAAA |
| 32 | 0.72 | 5:10:09.5 | -68:29:54.0 | 13.11 (0.02) | 12.74 (0.02) | 10.83 (0.01) | 9.06 (0.01) | 4.65 (0.02) | ··· | SMP33 | AAAAA |
| 33 | 0.31 | 5:10:17.2 | -68:48:22.5 | 14.06 (0.03) | 13.43 (0.02) | 12.96 (0.03) | 11.05 (0.02) | 5.92 (0.02) | ··· | SMP34 | AACCC |
| 34 | 0.76 | 5:10:50.0 | -65:29:30.4 | 15.23 (0.04) | 14.27 (0.03) | 13.90 (0.04) | 12.61 (0.03) | 6.90 (0.04) | ··· | SMP35 | AAAAA |
| 35 | 1.01 | 5:10:39.7 | -68:36:04.0 | 11.20 (0.01) | 10.63 (0.01) | 8.73 (0.00) | 6.89 (0.00) | 3.90 (0.02) | 1.97 (0.07) | SMP36 | CCBBB |
| 36 | 0.27 | 5:11:02.9 | -67:47:58.8 | 13.64 (0.02) | 13.06 (0.02) | 11.29 (0.01) | 9.49 (0.01) | 4.75 (0.01) | 3.15 (0.14) | SMP37 | AAAAA |
| 37 | 1.19 | 5:11:23.8 | -70:01:56.5 | 12.18 (0.01) | 11.71 (0.01) | 9.79 (0.01) | 7.76 (0.00) | 4.33 (0.01) | 2.89 (0.09) | SMP38 | AAAAA |
| 38 | 0.68 | 5:11:42.1 | -68:34:59.7 | 14.11 (0.03) | 13.58 (0.02) | 11.79 (0.01) | 9.89 (0.01) | 5.51 (0.03) | ··· | SMP39 | AACCA |
| 39 | 1.06 | 5:12:15.8 | -66:22:56.1 | 13.89 (0.02) | 13.28 (0.02) | 12.55 (0.02) | 11.25 (0.02) | 6.83 (0.03) | 3.26 (0.15) | SMP40 | AAAAA |
| 40 | 0.43 | 5:13:27.3 | -70:33:34.7 | 15.73 (0.06) | 14.89 (0.04) | ··· | 13.52 (0.06) | 7.30 (0.05) | ··· | SMP41 | AAAAA |
| 41 | 0.17 | 5:15:46.8 | -68:42:23.7 | 15.14 (0.04) | 14.37 (0.03) | 13.55 (0.04) | 11.73 (0.02) | 6.23 (0.03) | ··· | SMP42 | AAAAA |
| 43 | 0.91 | 5:18:29.9 | -67:16:55.8 | 15.32 (0.04) | 14.73 (0.04) | 13.90 (0.04) | 12.44 (0.03) | 7.58 (0.04) | ··· | SMP44 | CCBBA |
| 44 | 0.19 | 5:19:20.7 | -66:58:07.5 | 15.00 (0.04) | 14.04 (0.03) | 13.66 (0.04) | 12.16 (0.03) | 6.59 (0.02) | ··· | SMP45 | AAACA |
| 45 | 1.1 | 5:19:29.7 | -68:51:07.9 | 14.98 (0.04) | 14.88 (0.05) | 12.83 (0.02) | 10.95 (0.01) | 6.97 (0.03) | ··· | SMP46 | AAAAA |
| 46 | 0.66 | 5:19:54.7 | -69:31:04.5 | 13.03 (0.02) | 12.10 (0.01) | 10.64 (0.01) | 8.81 (0.01) | 3.40 (0.01) | ··· | SMP47 | BBCCA |
| 47 | 0.92 | 5:20:09.7 | -69:53:38.9 | 11.73 (0.01) | 11.22 (0.01) | 10.39 (0.01) | 8.84 (0.01) | 4.40 (0.01) | ··· | SMP48 | BBBBB |
| 48 | 0.23 | 5:20:09.4 | -70:25:38.1 | 16.39 (0.09) | 15.25 (0.06) | 15.83 (0.20) | 13.76 (0.07) | 8.02 (0.04) | ··· | SMP49 | AAAAA |
| 49 | 1.0 | 5:20:51.7 | -67:05:42.5 | 13.32 (0.02) | 12.54 (0.01) | 11.98 (0.01) | 10.40 (0.01) | 5.42 (0.02) | 3.38 (0.17) | SMP50 | AAAAA |
| 50 | 0.83 | 5:20:52.6 | -70:09:35.0 | 11.69 (0.01) | 10.74 (0.01) | 9.61 (0.01) | 7.54 (0.00) | 3.30 (0.01) | ··· | SMP51 | BBAAA |
| 51 | 0.67 | 5:21:23.8 | -68:35:34.4 | 14.25 (0.03) | 13.24 (0.02) | 12.85 (0.02) | 10.93 (0.01) | 5.10 (0.02) | ··· | SMP52 | AAAAA |
| 52 | 0.49 | 5:21:32.9 | -67:00:04.0 | 14.72 (0.03) | 13.98 (0.03) | 13.61 (0.03) | 11.80 (0.02) | 5.00 (0.02) | 2.48 (0.08) | SMP53 | AAAAA |
| 53 | 0.19 | 5:21:42.9 | -68:39:24.8 | 16.08 (0.07) | 15.12 (0.05) | 14.27 (0.06) | 12.78 (0.05) | 7.85 (0.04) | ··· | SMP54 | AAAAA |
| 54 | 0.2 | 5:22:41.0 | -71:19:06.7 | 12.48 (0.01) | 11.72 (0.01) | 10.52 (0.01) | 8.65 (0.00) | 4.15 (0.01) | 2.69 (0.07) | SMP55 | AAAEA |
| 55 | 0.46 | 5:23:31.2 | -69:04:04.4 | 13.20 (0.02) | 12.47 (0.01) | 11.77 (0.01) | 10.14 (0.01) | ··· | ··· | SMP56 | CCCCA |
| 56 | 0.7 | 5:23:48.6 | -69:12:21.6 | ··· | 14.58 (0.04) | ··· | ··· | 8.15 (0.05) | ··· | SMP57 | CCCCA |
| 57 | 1.15 | 5:24:20.9 | -70:05:00.5 | 12.16 (0.01) | 11.02 (0.01) | 9.87 (0.01) | 8.05 (0.00) | 3.99 (0.01) | ··· | SMP58 | AAAAA |
| 58 | 0.91 | 5:24:27.4 | -70:22:23.7 | 15.49 (0.05) | 14.60 (0.04) | 13.96 (0.04) | 12.71 (0.03) | 8.65 (0.05) | ··· | SMP59 | AAEEA |
| 59 | 0.28 | 5:24:15.7 | -70:53:56.3 | 14.98 (0.04) | 14.32 (0.03) | 13.22 (0.03) | 11.20 (0.01) | 6.66 (0.02) | ··· | SMP60 | CCCEA |

TABLE 3 —*Continued*

| LMC | Dist.[a] (arcsec) | R.A. (J2000) | Dec. (J2000) | [3.6] (err) | [4.5] (err) | [5.8] (err) | [8.0] (err) | [24] (err) | [70] (err) | Other names | Code[b] |
|---|---|---|---|---|---|---|---|---|---|---|---|
| 61 | 0.97 | 5:24:55.0 | -71:32:55.4 | 13.68 (0.02) | 12.60 (0.02) | 11.97 (0.02) | 9.83 (0.01) | 3.55 (0.01) | 2.05 (0.06) | SMP62 | AAAAA |
| 62 | 1.09 | 5:25:26.2 | -68:55:53.8 | 13.67 (0.02) | 12.81 (0.02) | 12.13 (0.02) | 10.28 (0.01) | 5.11 (0.02) | ··· | SMP63 | AAAAA |
| 63 | 0.88 | 5:27:35.8 | -69:08:56.3 | 9.88 (0.00) | 8.73 (0.00) | 7.82 (0.00) | 6.60 (0.00) | ··· | ··· | SMP64 | CCCBB |
| 64 | 0.47 | 5:27:43.8 | -71:25:56.0 | 14.67 (0.03) | 14.00 (0.03) | 13.33 (0.04) | 11.55 (0.02) | 7.54 (0.07) | ··· | SMP65 | AAAAA |
| 65 | 1.22 | 5:28:41.2 | -67:33:39.1 | 14.95 (0.04) | 14.20 (0.03) | 13.45 (0.03) | 11.55 (0.02) | 6.30 (0.03) | ··· | SMP66 | BBAAA |
| 66 | 0.67 | 5:29:15.7 | -67:32:46.7 | 14.74 (0.03) | 14.35 (0.03) | 12.88 (0.02) | 11.04 (0.01) | 5.71 (0.03) | ··· | SMP67 | AAAAA |
| 67 | 0.52 | 5:29:02.9 | -70:19:24.8 | 15.91 (0.08) | 14.30 (0.04) | 14.07 (0.05) | 12.67 (0.03) | 6.20 (0.03) | ··· | SMP68 | AAAAA |
| 68 | 0.61 | 5:29:23.2 | -67:13:21.9 | 16.40 (0.08) | 15.44 (0.06) | 14.62 (0.09) | 13.19 (0.06) | 8.00 (0.05) | ··· | SMP69 | AAAAA |
| 69 | 0.55 | 5:29:26.6 | -72:38:42.6 | 16.17 (0.07) | 15.28 (0.05) | 14.18 (0.05) | 13.11 (0.04) | 8.06 (0.05) | ··· | SMP70 | AAAAA |
| 70 | 0.43 | 5:30:33.3 | -70:44:37.6 | 12.83 (0.01) | 12.41 (0.01) | 10.65 (0.01) | 8.84 (0.01) | 4.53 (0.01) | ··· | SMP71 | AAAAA |
| 71 | 0.94 | 5:30:45.8 | -70:50:15.8 | 13.42 (0.02) | 13.59 (0.02) | 13.40 (0.03) | 13.17 (0.04) | 7.91 (0.04) | ··· | SMP72 | AAAAA |
| 72 | 0.92 | 5:31:22.0 | -70:40:44.9 | 12.35 (0.01) | 11.88 (0.01) | 10.23 (0.01) | 8.42 (0.00) | 4.22 (0.02) | ··· | SMP73 | AAAAA |
| 73 | 0.34 | 5:33:29.8 | -71:52:28.4 | 13.20 (0.02) | 12.53 (0.01) | 11.07 (0.01) | 9.10 (0.01) | 5.07 (0.02) | 3.26 (0.13) | SMP74 | AAAAA |
| 74 | 0.17 | 5:33:47.0 | -68:36:44.2 | 11.81 (0.01) | 11.29 (0.01) | 9.35 (0.00) | 7.46 (0.00) | 4.03 (0.01) | ··· | SMP75 | AAAAA |
| 75 | 0.79 | 5:33:56.2 | -67:53:08.3 | 13.26 (0.02) | 12.45 (0.01) | 10.95 (0.01) | 9.04 (0.01) | 4.68 (0.01) | ··· | SMP76 | AAAAA |
| 76 | 1.1 | 5:34:06.3 | -69:26:17.7 | 13.09 (0.02) | 12.37 (0.01) | 11.64 (0.01) | 9.96 (0.01) | 5.89 (0.03) | ··· | SMP77 | CCAAA |
| 77 | 0.62 | 5:34:21.3 | -68:58:24.9 | 12.73 (0.01) | 11.99 (0.01) | 10.39 (0.01) | 8.36 (0.00) | 4.02 (0.02) | ··· | SMP78 | AAAAA |
| 79 | 1.43 | 5:34:39.0 | -70:19:55.5 | 15.15 (0.04) | 14.71 (0.04) | ··· | 13.86 (0.08) | 8.98 (0.07) | ··· | SMP80 | CAAAA |
| 81 | 0.41 | 5:35:57.6 | -69:58:16.6 | 15.15 (0.04) | 14.36 (0.04) | 13.14 (0.03) | 11.40 (0.02) | 5.33 (0.02) | ··· | SMP82 | CCCCA |
| 82 | 0.21 | 5:36:20.8 | -67:18:07.5 | 14.73 (0.03) | 13.71 (0.02) | 13.53 (0.03) | 11.80 (0.02) | 5.22 (0.02) | ··· | SMP83 | AAAAA |
| 83 | 0.43 | 5:36:53.0 | -71:53:38.0 | 14.50 (0.03) | 13.41 (0.02) | ··· | 11.06 (0.01) | 6.15 (0.03) | ··· | SMP84 | AAAAA |
| 84 | 0.68 | 5:40:30.9 | -66:17:37.0 | 12.19 (0.01) | 11.41 (0.01) | 9.84 (0.01) | 8.01 (0.00) | 3.44 (0.02) | ··· | SMP85 | AAAAA |
| 85 | 0.54 | 5:41:22.1 | -68:07:44.2 | 16.56 (0.08) | 15.70 (0.07) | 15.03 (0.08) | 14.04 (0.07) | 9.03 (0.08) | ··· | SMP86 | AAAAA |
| 86 | 0.84 | 5:41:08.0 | -72:42:07.8 | 15.33 (0.04) | 14.44 (0.03) | 13.33 (0.03) | 11.80 (0.02) | ··· | 2.67 (0.10) | SMP87 | AAAEA |
| 87 | 0.56 | 5:42:33.3 | -70:29:24.0 | 13.33 (0.02) | 12.74 (0.02) | 12.46 (0.02) | 11.46 (0.02) | 7.47 (0.03) | ··· | SMP88 | AAAAA |
| 88 | 1.92 | 5:42:37.0 | -70:09:31.1 | 12.62 (0.01) | 12.26 (0.01) | 10.43 (0.01) | 8.80 (0.01) | 4.27 (0.01) | ··· | SMP89 | AAAAA |
| 89 | 0.9 | 5:44:34.8 | -70:21:40.0 | 13.35 (0.02) | 12.45 (0.01) | 11.62 (0.01) | 10.39 (0.01) | 7.08 (0.04) | ··· | SMP90 | AAAAA |
| 90 | 0.16 | 5:45:06.0 | -68:06:50.9 | 16.34 (0.07) | 15.47 (0.06) | ··· | 13.18 (0.05) | 8.45 (0.06) | ··· | SMP91 | AAAAA |
| 91 | 0.96 | 5:47:04.7 | -69:27:33.3 | 12.60 (0.01) | 12.10 (0.01) | 11.00 (0.01) | 9.31 (0.01) | 4.21 (0.01) | ··· | SMP92 | BBBBB |
| 92[d] | 0.94 | 5:49:38.8 | -69:09:59.3 | 14.72 (0.03) | 13.72 (0.02) | 12.10 (0.02) | 10.90 (0.02) | 8.09 (0.03) | ··· | SMP93 | EEEEE |
| 94 | 0.58 | 6:01:45.3 | -67:56:06.4 | 15.48 (0.05) | 15.08 (0.05) | 13.40 (0.03) | 11.66 (0.02) | 7.42 (0.04) | ··· | SMP95 | AAAAA |
| 102 | 1.56 | 4:24:37.6 | -69:42:20.7 | 12.47 (0.01) | 11.67 (0.01) | 11.38 (0.01) | 10.75 (0.01) | ··· | ··· | Sa104 | AAAAN |
| 103 | 0.69 | 5:02:32.9 | -69:26:15.2 | 16.30 (0.08) | 15.51 (0.06) | 14.19 (0.05) | 12.85 (0.04) | 9.09 (0.11) | ··· | Sa105 | AAAAB |
| 104 | 0.95 | 5:03:05.8 | -68:33:37.0 | 16.01 (0.06) | 15.86 (0.07) | 14.14 (0.05) | 12.33 (0.03) | 9.14 (0.08) | ··· | Sa106 | CCCAA |
| 105 | 1.13 | 5:06:43.7 | -69:15:37.8 | 15.53 (0.05) | 15.27 (0.06) | 14.50 (0.07) | 13.02 (0.05) | 8.43 (0.04) | ··· | Sa107 | CCCAA |
| 106 | 1.26 | 5:11:48.1 | -69:23:43.1 | 11.85 (0.01) | 11.12 (0.01) | 10.52 (0.01) | 9.37 (0.01) | 6.22 (0.04) | ··· | Sa109 | AAAAA |
| 107 | 1.05 | 5:12:16.7 | -68:29:10.1 | ··· | 16.96 (0.15) | ··· | ··· | 10.20 (0.18) | ··· | Sa110 | NNNNN |
| 108 | 0.36 | 5:24:56.7 | -69:15:31.2 | 15.69 (0.06) | 14.50 (0.04) | 13.69 (0.06) | 11.66 (0.04) | 6.51 (0.03) | ··· | Sa117 | AAACC |
| 109 | 0.31 | 5:29:32.7 | -70:17:39.0 | ··· | 16.17 (0.09) | ··· | 13.24 (0.05) | 9.10 (0.07) | ··· | Sa120 | NNAAA |
| 110 | 0.66 | 5:30:26.3 | -71:13:48.0 | 17.81 (0.17) | 17.15 (0.14) | ··· | ··· | ··· | ··· | Sa121 | NNNNN |
| 111 | 0.67 | 5:34:24.3 | -69:34:28.0 | ··· | 15.65 (0.07) | 15.66 (0.21) | ··· | 7.33 (0.04) | ··· | Sa122 | NNNNC |
| 112 | 0.35 | 5:34:30.2 | -70:28:34.5 | 15.32 (0.05) | 14.70 (0.04) | 13.31 (0.03) | 11.46 (0.02) | 6.71 (0.03) | ··· | Sa123 | AAAAA |
| 113 | 0.68 | 5:40:44.6 | -67:18:07.7 | 16.51 (0.08) | 15.66 (0.06) | 14.55 (0.07) | 13.00 (0.04) | 8.94 (0.07) | ··· | Sa124 | AAAAA |
| 114 | 0.58 | 5:53:14.6 | -70:25:02.0 | 15.81 (0.06) | 15.67 (0.06) | 14.40 (0.06) | 12.70 (0.03) | 8.46 (0.06) | ··· | Sa126 | AAAAA |
| 118 | 0.44 | 5:12:59.9 | -68:57:07.7 | 18.41 (0.37) | 17.38 (0.22) | ··· | ··· | 9.78 (0.12) | ··· | J10 | NNNNA |
| 120 | 0.94 | 5:15:08.7 | -69:21:00.9 | ··· | ··· | ··· | 13.37 (0.07) | 9.95 (0.16) | ··· | J14 | NNNCC |
| 123 | 1.48 | 5:17:00.7 | -69:19:29.1 | 8.96 (0.00) | 8.05 (0.00) | 7.43 (0.00) | 6.53 (0.00) | 4.39 (0.01) | ··· | J17 | AAAAA |
| 124 | 0.46 | 5:17:23.9 | -69:39:13.2 | 15.83 (0.07) | ··· | ··· | ··· | ··· | ··· | J18 | NNNNN |
| 125 | 0.38 | 5:17:58.9 | -69:39:23.0 | 8.31 (0.00) | 8.19 (0.00) | 7.83 (0.00) | 7.59 (0.00) | 5.59 (0.02) | ··· | J19 | CCCCC |
| 126 | 1.1 | 5:18:45.8 | -69:10:11.5 | 15.73 (0.07) | ··· | ··· | ··· | ··· | ··· | Sa112 | NNNNN |
| 127 | 0.22 | 5:18:55.7 | -69:33:02.1 | 13.60 (0.02) | 13.81 (0.03) | 13.81 (0.05) | 13.88 (0.16) | 9.84 (0.13) | ··· | J21 | AAAAN |
| 128 | 0.85 | 5:19:07.0 | -69:41:54.0 | 12.79 (0.01) | 12.82 (0.02) | 12.71 (0.02) | 12.22 (0.03) | 8.35 (0.06) | ··· | J22 | CCCCC |
| 129 | 0.26 | 5:19:15.1 | -69:34:52.6 | 15.59 (0.08) | 15.68 (0.09) | ··· | ··· | ··· | ··· | J23 | AACCC |
| 132 | 0.17 | 5:20:56.9 | -70:05:10.5 | 13.56 (0.02) | 13.65 (0.03) | 13.50 (0.04) | ··· | ··· | ··· | Sa114 | mis-ID? |
| 133 | 1.9 | 5:21:07.6 | -69:44:28.1 | ··· | 16.01 (0.13) | 14.65 (0.09) | 12.49 (0.03) | 9.27 (0.09) | ··· | J32 | NNAAC |

TABLE 3 —*Continued*

| LMC | Dist.[a] (arcsec) | R.A. (J2000) | Dec. (J2000) | [3.6] (err) | [4.5] (err) | [5.8] (err) | [8.0] (err) | [24] (err) | [70] (err) | Other names | Code[b] |
|---|---|---|---|---|---|---|---|---|---|---|---|
| 134 | 1.48 | 5:21:17.6 | -69:43:01.0 | ··· | ··· | ··· | 12.66 (0.07) | 7.54 (0.04) | ··· | Sa115 | NNNCB |
| 135 | 1.44 | 5:24:36.6 | -69:05:51.1 | 15.42 (0.05) | 14.87 (0.04) | 14.01 (0.05) | 12.88 (0.05) | 8.44 (0.05) | ··· | Sa116 | AAAAA |
| 136 | 1.66 | 5:26:09.5 | -69:00:58.5 | 15.22 (0.04) | 15.06 (0.05) | ··· | ··· | 8.66 (0.06) | ··· | Sa118 | BBAAA |
| 137 | 0.93 | 4:47:22.8 | -67:41:18.8 | ··· | 16.57 (0.10) | ··· | ··· | ··· | ··· | MG01 | NNNNN |
| 138 | 0.89 | 4:48:09.3 | -68:33:39.0 | 16.52 (0.08) | 15.74 (0.07) | 14.42 (0.06) | 13.07 (0.04) | ··· | ··· | MG02 | AAAAA |
| 139 | 0.83 | 4:50:56.7 | -66:19:52.5 | 16.99 (0.10) | 16.71 (0.11) | ··· | 13.13 (0.04) | 10.26 (0.17) | ··· | MG03 | NNAAN |
| 140 | 0.72 | 4:52:45.2 | -70:17:49.1 | ··· | 16.40 (0.10) | ··· | ··· | ··· | ··· | MG04 | NNAAN |
| 141 | 0.69 | 4:53:29.7 | -68:22:52.3 | 17.87 (0.20) | 16.79 (0.13) | ··· | ··· | 9.24 (0.08) | ··· | MG05 | NNNAA |
| 144 | 1.28 | 4:55:39.8 | -68:34:20.3 | 17.28 (0.14) | 16.18 (0.09) | ··· | 13.99 (0.17) | 9.50 (0.10) | ··· | MG08 | NNAAA |
| 145 | 1.56 | 4:56:21.1 | -67:24:22.5 | 16.81 (0.10) | 16.05 (0.08) | 14.63 (0.07) | ··· | ··· | ··· | MG09 | NNAAN |
| 146 | 1.11 | 4:56:37.8 | -67:40:54.6 | 16.46 (0.08) | 16.28 (0.09) | 14.18 (0.05) | 12.30 (0.03) | 9.05 (0.07) | ··· | MG10 | AAAAA |
| 147 | 0.66 | 4:59:18.3 | -67:27:03.9 | 17.15 (0.12) | 16.41 (0.10) | ··· | ··· | 8.40 (0.05) | ··· | MG11 | NNNAA |
| 148 | 0.92 | 5:01:40.3 | -66:46:45.6 | ··· | 17.28 (0.16) | ··· | ··· | ··· | ··· | MG12 | NNNNN |
| 149 | 0.57 | 5:03:03.3 | -65:23:02.3 | 18.22 (0.20) | 16.93 (0.12) | ··· | 14.61 (0.11) | 10.17 (0.16) | ··· | MG13 | NNNNN |
| 150 | 0.52 | 5:04:27.7 | -68:58:11.4 | 15.35 (0.05) | 14.67 (0.04) | 13.75 (0.05) | 11.65 (0.03) | 7.31 (0.03) | ··· | MG14 | CCCCC |
| 151 | 1.31 | 5:05:35.7 | -68:01:40.1 | 16.71 (0.09) | 16.25 (0.09) | ··· | ··· | ··· | ··· | MG15 | NNNEN |
| 152 | 0.06 | 5:06:05.2 | -64:48:49.2 | 16.80 (0.09) | 15.97 (0.07) | ··· | ··· | ··· | ··· | MG16 | AAAAA |
| 153 | 0.39 | 5:06:21.2 | -64:37:03.5 | 17.19 (0.11) | 16.67 (0.11) | 14.81 (0.08) | 13.28 (0.04) | 8.33 (0.06) | ··· | MG17 | AAAAA |
| 155 | 0.97 | 5:08:32.0 | -68:09:44.3 | 17.19 (0.12) | 16.60 (0.11) | ··· | 13.42 (0.06) | ··· | ··· | MG19 | CCCCN |
| 156 | 0.5 | 5:10:40.2 | -68:10:23.5 | 17.26 (0.12) | 16.70 (0.11) | ··· | ··· | ··· | ··· | MG20 | NNNNN |
| 157 | 0.84 | 5:11:38.0 | -65:42:42.1 | 16.88 (0.09) | 15.77 (0.07) | ··· | ··· | 7.78 (0.04) | ··· | MG21 | NAAAA |
| 158 | 0.98 | 5:11:53.5 | -65:32:27.0 | 18.16 (0.20) | 17.48 (0.18) | ··· | ··· | 9.56 (0.11) | ··· | MG22 | NNNNA |
| 159 | 0.85 | 5:11:47.4 | -68:16:09.5 | 16.72 (0.09) | 16.25 (0.09) | ··· | 13.54 (0.07) | 8.47 (0.05) | ··· | MG23 | CCCCA |
| 160 | 0.06 | 5:13:01.0 | -65:15:34.1 | 18.02 (0.18) | ··· | ··· | 15.49 (0.25) | ··· | ··· | MG24 | NNNNN |
| 161 | 0.79 | 5:12:17.8 | -71:54:49.5 | 17.46 (0.13) | 16.83 (0.12) | ··· | ··· | ··· | ··· | MG25 | AANNN |
| 162 | 0.46 | 5:13:28.0 | -66:17:28.4 | 13.28 (0.02) | 12.51 (0.01) | 11.23 (0.01) | 9.18 (0.01) | 5.09 (0.03) | ··· | MG26 | AAAAA |
| 163 | 0.29 | 5:13:34.2 | -65:35:13.2 | 17.83 (0.16) | ··· | ··· | ··· | 9.91 (0.13) | ··· | MG27 | NNNNN |
| 164 | 0.48 | 5:13:09.7 | -69:31:18.0 | ··· | ··· | ··· | 14.62 (0.19) | 9.91 (0.16) | ··· | MG28 | CCCCC |
| 165 | 0.88 | 5:13:42.4 | -68:15:16.4 | 16.34 (0.08) | 15.58 (0.07) | ··· | ··· | 7.68 (0.04) | ··· | MG29 | CAAAC |
| 166 | 0.32 | 5:14:14.7 | -70:50:31.5 | 16.20 (0.07) | 15.27 (0.06) | 14.70 (0.08) | 12.77 (0.03) | 7.21 (0.03) | ··· | MG30 | CCAAA |
| 167 | 0.75 | 5:16:29.3 | -68:18:11.3 | 16.67 (0.09) | 16.20 (0.09) | 14.62 (0.08) | 12.83 (0.04) | 8.93 (0.06) | ··· | MG31 | CCCAA |
| 168 | 0.4 | 5:19:04.0 | -64:59:18.6 | 16.19 (0.07) | 15.55 (0.06) | ··· | 13.57 (0.06) | ··· | ··· | MG32 | AAAAN |
| 169 | 1.11 | 5:19:13.7 | -66:09:31.3 | 18.00 (0.18) | 17.18 (0.14) | 16.65 (0.37) | 14.64 (0.12) | 10.52 (0.24) | ··· | MG33 | NNNEA |
| 170 | 0.61 | 5:19:28.9 | -67:14:26.5 | 16.22 (0.07) | 15.47 (0.06) | 13.97 (0.05) | 12.08 (0.02) | 8.07 (0.05) | ··· | MG34 | AAAAA |
| 171 | 0.47 | 5:19:33.4 | -66:55:37.2 | 11.26 (0.01) | 10.38 (0.01) | 9.71 (0.01) | 8.68 (0.00) | 6.04 (0.03) | ··· | MG35 | AAAAA |
| 172 | 0.9 | 5:20:29.7 | -64:53:14.0 | 16.51 (0.08) | 15.53 (0.06) | ··· | 13.16 (0.04) | ··· | ··· | MG36 | EEEEA |
| 173 | 0.46 | 5:21:46.8 | -65:22:26.7 | 15.77 (0.06) | 15.18 (0.05) | 14.43 (0.06) | 12.68 (0.03) | 8.33 (0.05) | ··· | MG37 | AAAAA |
| 174 | 0.65 | 5:22:03.0 | -64:25:16.0 | 17.49 (0.14) | ··· | ··· | ··· | ··· | ··· | MG38 | NNNAA |
| 175 | 0.63 | 5:22:12.9 | -69:43:29.1 | 12.42 (0.01) | 11.15 (0.01) | 9.92 (0.01) | 8.30 (0.01) | 3.50 (0.01) | ··· | MG39 | AACCC |
| 176 | 0.62 | 5:22:35.3 | -68:24:25.3 | 15.72 (0.06) | 14.90 (0.04) | 14.19 (0.06) | 12.17 (0.03) | 7.03 (0.03) | ··· | MG40 | CCCCA |
| 177 | 0.61 | 5:23:37.7 | -65:09:54.3 | 16.41 (0.07) | 16.21 (0.08) | 13.97 (0.04) | 12.16 (0.02) | 9.16 (0.09) | ··· | MG41 | AAAAA |
| 179 | 0.1 | 5:24:34.2 | -71:13:39.5 | ··· | 16.46 (0.10) | ··· | 14.13 (0.09) | 8.41 (0.06) | ··· | MG43 | NNNAA |
| 182 | 0.9 | 5:26:20.5 | -65:21:45.9 | 14.33 (0.03) | 13.96 (0.03) | 13.73 (0.04) | 13.13 (0.04) | ··· | ··· | MG46 | AAAAA |
| 183 | 1.8 | 5:26:45.3 | -64:38:00.8 | 14.87 (0.04) | 13.87 (0.03) | 12.73 (0.02) | 10.31 (0.01) | 8.98 (0.07) | ··· | MG47 | AAAAA |
| 184 | 0.76 | 5:26:59.8 | -66:07:05.8 | 17.27 (0.11) | 16.50 (0.10) | ··· | 13.50 (0.05) | 9.01 (0.08) | ··· | MG48 | AANAA |
| 185 | 0.08 | 5:27:32.1 | -69:32:18.8 | 15.75 (0.06) | 14.92 (0.05) | 14.43 (0.06) | 12.61 (0.03) | 7.11 (0.03) | ··· | MG49 | CCCAA |
| 186 | 0.21 | 5:29:08.6 | -66:42:56.3 | 17.80 (0.16) | 16.12 (0.08) | ··· | ··· | 7.56 (0.04) | ··· | MG50 | NANAA |
| 187 | 0.22 | 5:28:34.4 | -70:33:01.6 | 15.23 (0.04) | 14.93 (0.05) | ··· | 12.62 (0.03) | 9.15 (0.10) | ··· | MG51 | CCAAA |
| 188 | 0.54 | 5:29:08.8 | -69:45:28.0 | 16.15 (0.08) | 15.78 (0.08) | 14.31 (0.06) | 12.54 (0.03) | 8.24 (0.05) | ··· | MG52 | CCAAA |
| 189 | 0.78 | 5:29:35.7 | -69:46:05.2 | ··· | 15.30 (0.06) | ··· | ··· | 9.35 (0.10) | ··· | MG53 | CCCCA |
| 190 | 0.69 | 5:29:51.4 | -68:50:05.6 | 16.03 (0.06) | 15.57 (0.06) | ··· | 12.88 (0.04) | ··· | ··· | MG54 | CCCAN |
| 191 | 1.1 | 5:31:09.1 | -71:36:40.2 | ··· | 15.73 (0.07) | ··· | ··· | 8.53 (0.05) | ··· | MG55 | CCNAA |
| 194 | 0.29 | 5:32:37.7 | -67:08:31.1 | 17.34 (0.12) | 16.66 (0.11) | ··· | ··· | ··· | ··· | MG58 | NNNNN |
| 195 | 0.48 | 5:32:56.0 | -65:16:42.0 | 14.73 (0.03) | 14.11 (0.03) | 13.27 (0.03) | 12.90 (0.03) | 9.31 (0.07) | ··· | MG59 | AAAAA |
| 196 | 0.57 | 5:33:30.9 | -69:08:13.3 | 16.11 (0.07) | 15.51 (0.06) | ··· | 12.82 (0.06) | 9.29 (0.10) | ··· | MG60 | CCCCC |

TABLE 3 —*Continued*

| LMC | Dist.[a] (arcsec) | R.A. (J2000) | Dec. (J2000) | [3.6] (err) | [4.5] (err) | [5.8] (err) | [8.0] (err) | [24] (err) | [70] (err) | Other names | Code[b] |
|---|---|---|---|---|---|---|---|---|---|---|---|
| 197 | 0.99 | 5:33:13.1 | -72:36:46.3 | 17.34 (0.12) | 16.52 (0.10) | ··· | 13.89 (0.07) | 9.04 (0.06) | ··· | MG61 | NNNAC |
| 198 | 1.25 | 5:34:36.5 | -68:18:27.9 | 16.27 (0.09) | 16.24 (0.10) | ··· | ··· | ··· | ··· | MG62 | CCCCC |
| 199 | 0.66 | 5:34:10.2 | -71:43:14.1 | 15.61 (0.05) | 15.51 (0.06) | ··· | ··· | ··· | ··· | MG63 | CCNNN |
| 200 | 1.86 | 5:35:12.8 | -67:37:58.0 | 16.44 (0.09) | 15.95 (0.08) | ··· | ··· | 9.39 (0.11) | ··· | MG64 | AACCC |
| 201 | 1.42 | 5:35:10.3 | -69:39:38.9 | 15.92 (0.07) | 14.74 (0.04) | ··· | 12.53 (0.07) | 6.74 (0.03) | ··· | MG65 | CCCCC |
| 202 | 0.33 | 5:37:59.5 | -65:58:50.0 | 16.96 (0.10) | 16.56 (0.10) | 14.83 (0.08) | ··· | ··· | ··· | MG66 | NAAAN |
| 203 | 0.63 | 5:37:38.0 | -71:41:37.9 | ··· | 16.58 (0.11) | ··· | ··· | 9.14 (0.07) | ··· | MG67 | NNNAA |
| 204 | 0.49 | 5:38:19.5 | -68:58:37.2 | 15.49 (0.05) | 15.12 (0.05) | ··· | 11.77 (0.04) | 8.03 (0.05) | ··· | MG68 | CCCCC |
| 205 | 1.42 | 5:39:15.5 | -66:49:43.5 | 18.00 (0.18) | 17.08 (0.14) | ··· | ··· | ··· | ··· | MG69 | NNNNN |
| 207 | 0.97 | 5:39:54.9 | -66:34:13.1 | 17.05 (0.11) | 16.33 (0.09) | ··· | ··· | 9.45 (0.14) | ··· | MG71 | NAANA |
| 208 | 1.3 | 5:40:20.3 | -67:02:02.1 | ··· | 16.47 (0.10) | ··· | 14.35 (0.11) | 10.01 (0.16) | ··· | MG72 | NNNAA |
| 211 | 1.97 | 5:42:15.4 | -68:48:55.7 | 17.16 (0.12) | ··· | ··· | ··· | ··· | ··· | MG75 | NNNNN |
| 212 | 0.75 | 5:42:24.2 | -69:53:05.1 | 16.13 (0.07) | 15.58 (0.07) | 15.50 (0.17) | 13.27 (0.07) | 7.85 (0.04) | ··· | MG76 | CCCAA |
| 213 | 1.56 | 5:43:47.6 | -68:38:35.1 | 17.81 (0.18) | 16.30 (0.09) | ··· | ··· | 10.22 (0.20) | ··· | MG77 | NNCCC |
| 214 | 0.29 | 5:46:25.4 | -67:50:02.8 | 17.07 (0.11) | 16.12 (0.08) | ··· | ··· | ··· | ··· | Mo40 | NACAN |
| 215 | 0.59 | 5:45:59.7 | -71:19:04.9 | 13.34 (0.02) | 13.39 (0.02) | 13.41 (0.03) | 13.41 (0.06) | ··· | ··· | MG79 | CCCCC |
| 217 | 0.31 | 5:51:00.1 | -67:58:45.6 | 17.38 (0.12) | 16.35 (0.09) | ··· | ··· | ··· | ··· | MG81 | NNNEN |
| 218 | 0.73 | 5:53:11.9 | -71:28:57.0 | 16.46 (0.08) | 15.82 (0.08) | ··· | ··· | ··· | ··· | MG82 | AANAN |
| 224 | 1.69 | 4:34:46.7 | -69:23:19.6 | ··· | 16.73 (0.11) | ··· | ··· | ··· | ··· | Mo2 | NNNAN |
| 225 | 1.17 | 4:36:14.4 | -70:31:03.0 | 18.20 (0.19) | ··· | ··· | ··· | ··· | ··· | Mo3 | NNNNN |
| 227 | 0.88 | 4:45:19.9 | -67:34:33.4 | 17.44 (0.13) | 16.61 (0.11) | ··· | 14.39 (0.09) | ··· | ··· | Mo5 | NNNEN |
| 228 | 0.83 | 4:46:33.1 | -70:12:46.4 | 17.27 (0.12) | 16.51 (0.10) | 15.34 (0.12) | 13.53 (0.05) | 9.31 (0.08) | ··· | Mo6 | AAAAA |
| 231 | 1.98 | 4:52:11.4 | -70:12:46.4 | 10.22 (0.00) | 9.44 (0.00) | 8.86 (0.00) | 8.03 (0.00) | 5.84 (0.03) | ··· | Mo9 | AAAAA |
| 232 | 0.39 | 4:55:45.4 | -65:48:34.7 | 17.10 (0.11) | 16.68 (0.11) | 14.90 (0.08) | 13.23 (0.04) | 8.74 (0.06) | ··· | Mo10 | AAAAA |
| 233 | 0.61 | 4:58:03.2 | -70:25:08.8 | 16.83 (0.09) | 15.99 (0.07) | 14.72 (0.07) | 13.28 (0.04) | ··· | ··· | Mo11 | AAAAA |
| 234 | 0.42 | 4:58:37.0 | -69:35:46.5 | ··· | 15.42 (0.06) | ··· | 13.18 (0.04) | ··· | ··· | Mo12 | CCCCN |
| 238 | 0.78 | 5:06:14.9 | -69:48:24.7 | ··· | 14.93 (0.05) | 14.19 (0.05) | 13.16 (0.05) | ··· | ··· | Mo16 | CCCCA |
| 239 | 0.69 | 5:07:25.5 | -67:28:49.5 | 16.68 (0.09) | 15.95 (0.07) | 14.55 (0.06) | 13.33 (0.05) | ··· | ··· | Mo17 | CCAAN |
| 240 | 0.91 | 5:09:11.2 | -67:34:01.7 | 15.75 (0.06) | 15.12 (0.05) | ··· | 12.60 (0.03) | 7.99 (0.04) | ··· | Mo18 | AAAAA |
| 241 | 0.76 | 5:11:00.5 | -70:05:04.8 | 16.92 (0.11) | 16.33 (0.10) | ··· | 13.63 (0.06) | 8.69 (0.06) | ··· | Mo19 | CCCAA |
| 242 | 0.89 | 5:11:10.8 | -71:10:26.4 | ··· | 16.04 (0.08) | ··· | ··· | ··· | ··· | Mo20 | NNNAA |
| 243 | 0.21 | 5:19:04.1 | -64:44:38.1 | ··· | 16.41 (0.09) | ··· | ··· | ··· | ··· | Mo21 | NAAAN |
| 245 | 1.45 | 5:21:52.3 | -69:43:18.0 | 16.16 (0.10) | ··· | ··· | ··· | ··· | ··· | Mo23 | CCCCC |
| 246 | 0.33 | 5:22:53.2 | -71:05:40.7 | 16.85 (0.10) | 16.03 (0.08) | 14.78 (0.08) | 13.09 (0.04) | 9.22 (0.09) | ··· | Mo24 | CAAAA |
| 247 | 0.67 | 5:26:02.6 | -72:31:02.5 | 17.00 (0.10) | 16.17 (0.08) | 14.79 (0.07) | 13.54 (0.05) | ··· | ··· | Mo25 | AAAAA |
| 248 | 1.73 | 5:28:01.5 | -70:13:30.1 | ··· | ··· | ··· | 12.86 (0.08) | 8.78 (0.08) | ··· | Mo26 | CCCCC |
| 249 | 0.98 | 5:29:16.7 | -69:37:18.1 | 14.88 (0.04) | 14.75 (0.04) | 14.11 (0.06) | 12.80 (0.04) | 9.75 (0.19) | ··· | Mo27 | CCCCC |
| 250 | 0.96 | 5:29:18.4 | -70:23:49.7 | 14.46 (0.03) | 14.70 (0.04) | 13.74 (0.04) | 12.21 (0.03) | 8.10 (0.04) | ··· | Mo28 | CCCCA |
| 252 | 0.84 | 5:31:35.3 | -69:23:46.4 | 17.11 (0.15) | ··· | ··· | ··· | 9.84 (0.16) | ··· | Mo30 | NNNNC |
| 254 | 0.39 | 5:32:05.2 | -69:57:27.4 | ··· | 15.72 (0.07) | ··· | ··· | ··· | ··· | Mo32 | CCAAN |
| 255 | 0.98 | 5:32:09.3 | -70:24:41.5 | 13.74 (0.02) | ··· | ··· | ··· | 9.29 (0.08) | ··· | Mo33 | CCCCC |
| 258 | 1.26 | 5:38:53.6 | -69:57:55.7 | 14.93 (0.04) | 15.16 (0.06) | ··· | 12.71 (0.10) | ··· | ··· | Mo36 | CCCCC |
| 259 | 0.51 | 5:39:14.5 | -70:00:18.6 | 15.84 (0.07) | 15.49 (0.06) | 13.36 (0.04) | ··· | ··· | ··· | Mo37 | CCCCC |
| 260 | 0.82 | 5:40:32.3 | -68:44:47.6 | 16.51 (0.08) | 15.69 (0.07) | ··· | 12.89 (0.05) | 9.80 (0.15) | ··· | Mo38 | CCCCC |
| 261 | 0.63 | 5:42:41.1 | -70:05:49.1 | 16.78 (0.10) | 15.72 (0.07) | ··· | ··· | ··· | ··· | Mo39 | NACCC |
| 262 | 0.71 | 5:46:25.3 | -71:23:22.3 | 17.12 (0.11) | 16.19 (0.09) | ··· | 14.15 (0.09) | ··· | ··· | Mo40 | CCCAA |
| 264 | 0.54 | 5:55:14.6 | -66:50:24.6 | 16.67 (0.09) | 15.76 (0.07) | ··· | 13.69 (0.06) | 9.44 (0.09) | ··· | Mo42 | AACAA |
| 266 | 1.32 | 6:01:43.3 | -68:00:35.0 | ··· | 16.12 (0.08) | ··· | ··· | ··· | ··· | Mo44 | CCAAN |
| 277 | 0.32 | 5:07:30.8 | -69:08:07.0 | ··· | ··· | ··· | 9.29 (0.01) | 4.18 (0.02) | ··· | SMP26 | CCCCA |

TABLE 3 —*Continued*

| LMC | Dist.[a] (arcsec) | R.A. (J2000) | Dec. (J2000) | [3.6] (err) | [4.5] (err) | [5.8] (err) | [8.0] (err) | [24] (err) | [70] (err) | Other names | Code[b] |
|---|---|---|---|---|---|---|---|---|---|---|---|

[a] Distance in arcsec between the position determined from the 3.6 $\mu$m photometry and the Leisy et al. (1997) catalog position.

[b] Characteristics of the source and field near the nebula. A=well defined, isolated point source, B=blended with other nearby point source, C=complex background or distribution of many nearby point sources, E=extended source, N=no source visible or too faint to determine whether extended or pointlike.

[c] The source identifications given by Leisy et al. (1997) for the objects in their catalog. Abbreviations are J: Jacoby Jacoby (1980), MG: Morgan & Good (1992), Mo: Morgan (1994), Sa: Sanduleak (1984), SMP: Sanduleak et al. (1978).

[d] Because it is extended in the IRAC images, the photometry for LMC 92 (SMP 93) was performed by summing the flux above the background in a $25.''62 \times 17.''08$ box centered on the core.